Accurate Vibrational-Rotational Parameters and Infrared Intensities of 1-Bromo-1-Fluoroethene: a Joint Experimental Analysis and *Ab Initio* Study

Andrea Pietropolli Charmet,[a,*] Paolo Stoppa,[a] Santi Giorgianni,[a] Julien Bloino,[b] Nicola Tasinato,[c] Ivan Carnimeo,[c,d] Malgorzata Biczysko,[e] Cristina Puzzarini[f]

[a]Dipartimento di Scienze Molecolari e Nanosistemi, Università Ca' Foscari Venezia, Via Torino 155, I-30172 Mestre (Ve), Italy.

[b]Consiglio Nazionale delle Ricerche, Istituto di Chimica dei Composti OrganoMetallici (ICCOM-CNR), UOS di Pisa, Area della Ricerca CNR, Via G. Moruzzi 1, I-56124 Pisa, Italy

[c]Scuola Normale Superiore, Piazza dei Cavalieri 7, I-56126 Pisa, Italy.

[d]Present address: Scuola Internazionale di Studi Avanzati (SISSA), via Bonomea, 265, I-34136 Trieste, Italy.

[e]International Centre for Quantum and Molecular Structures (ICQMS), College of Sciences, Shanghai University, 99 Shangda Road, 200444 Shanghai, China.

[f]Dipartimento di Chimica "Giacomo Giamician", Università di Bologna, Via Selmi 2, I-40126, Bologna, Italy.

[*]corresponding author (Tel: +39 041 2348541; Email: jacpnike@unive.it)

ABSTRACT

The medium-resolution gas-phase infrared (IR) spectra of 1-bromo-1-fluoroethene ($BrFC=CH_2$, 1,1-C_2H_2BrF) were investigated in the range 300 – 6500 cm^{-1}, and the vibrational analysis led to the assignment of all fundamentals as well as many overtone and combination bands up to three quanta, thus giving an accurate description of its vibrational structure. Integrated band intensity data were determined with high precision from the measurements of their corresponding absorption cross sections. The vibrational analysis was supported by high-level *ab initio* investigations. CCSD(T) computations accounting for extrapolation to the complete basis set and core correlation effects were employed to accurately determine the molecular structure and harmonic force field. The latter was then coupled to B2PLYP and MP2 computations in order to account for mechanical and electrical anharmonicities. Second-order perturbative vibrational theory was then applied to the hybrid force fields so obtained to support the experimental assignment of the IR spectra.

1. INTRODUCTION

Many of the experimental and theoretical investigations carried out on halogenated ethenes in the last decade were motivated by their role played as organic trace gas pollutants.[1-3] Besides their threats to human health, the brominated ones (mainly used in industry as intermediates in the production of polymers and pharmaceutical products, as components of fire extinguishers in blends with fluorine-containing compounds, and in the synthesis of copolymers having flame-retardant properties)[4] rise additional concerns in view of their high efficiency at catalyzing the destruction of the Earth's protective ozone layer.[5–9] Among the different techniques available for environmental monitoring, infrared (IR) spectroscopy is one of the most effective;[10] however, its performances rely strongly on the availability of sufficiently accurate spectroscopic data. These are provided by high-resolution studies, which are, however, often complicated by spectral congestion (due to the presence of different isotopomers and several hot bands) and many interacting vibrational levels. The huge challenge represented by the analysis of these spectra is nowadays faced with the help of a joint effort of experimental techniques, data-processing procedures, and *ab initio* calculations. Techniques like supersonic-jet expansions[11–15] and cell cooling[16–19] are able to significantly reduce the spectral congestion while keeping an adequate signal-to-noise ratio (SNR) in the measured signals thus facilitating the spectral assignments. *Ad-hoc* data-processing methodologies[20–27] developed for assisting the assignments and fitting procedure greatly simplify a large number of tasks that otherwise would be very difficult and time-consuming. *Ab initio* calculations are able to properly model all possible resonances affecting the vibrational levels, thus providing the basic spectroscopic data needed to support and guide the rovibrational analysis.[28–40]

Besides their impact on the environment, short-chain organic compounds, like halogenated ethenes, are thoroughly investigated to benchmark the performances of theoretical methods for deriving equilibrium structures,[41,42] thermochemical data,[43] stabilities,[44,45] and centrifugal distortion constants.[46] Furthermore, recent studies have also focused on disentangling polyads showing

several anharmonic resonances among different vibrational states.[47–51] Not to mention that their reactivity related to the presence of the carbon-carbon double bond prompted studies concerning the different steps involved in their photo-degradation.[52–55]

Among the different classes of halogenated ethenes, those containing bromine atoms show additional complexity in the analysis of their spectra due to several hot bands from the low-lying vibrational states, the concomitant presence of two isotopologues with an almost equal isotopic ratio, and small values of the rotational constants. All these factors hamper the high-resolution rovibrational analysis, which, in turn, is needed to determine the molecular constants with the accuracy required for detection by IR techniques. Concerning 1-bromo-1-fluoroethene ($BrFC=CH_2$, C_2H_2BrF), to our knowledge, the only spectroscopic characterization available in the literature is the microwave study carried out by Shimada et *al.*,[56] which led to the determination of its molecular structure, nuclear quadrupole coupling constants, rotational constants and quartic centrifugal distortion terms. Additionally, its adsorption on TiO2 has also been investigated.[57]

In the present contribution, we report on a joint experimental-computational study of 1-bromo-1-fluoroethene. Its vibrational spectrum was thoroughly analyzed and, in addition to all fundamentals, the most important spectral absorptions falling in the 300 – 6500 cm^{-1} region were assigned in terms of overtones, combination and hot bands up to three quanta. The vibrational analysis of the infrared spectra was assisted by high-level quantum-chemical calculations performed at different levels of theory, both involving post-Hartree-Fock methods and Density Functional Theory (DFT). In particular, an accurate description of the harmonic force field was obtained by means of a composite scheme including a highly correlated treatment of the electronic structure at the coupled-cluster (CC) level as well as an extrapolation to the complete basis-set limit and core-correlation effects.[37,58] In our description, anharmonicity was then taken into account by setting up hybrid force fields starting from the harmonic force field mentioned above and incorporating cubic and semi-diagonal quartic force constants at either the DFT level using the double-hybrid B2PLYP functional,[59] or evaluated by second-order Møller-Plesset theory (MP2).[60] Subsequently, second-

order vibrational perturbation theory (VPT2)[61-64] was considered to predict vibrational transition energies and intensities, in both cases also accounting for anharmonic resonances.[65-67]

2. EXPERIMENTAL AND COMPUTATIONAL DETAILS

2.1 Experimental details.

For recording the gas-phase infrared spectra used in the vibrational analysis, two different FTIR spectrometers were employed according to the spectral region. The measurements between 200 and 400 cm^{-1} were carried out at a resolution of 1.0 cm^{-1} by using a Nicolet Magna 750 (Perkin Elmer) spectrometer and employing a cell, fitted with KRS-5 window, with an optical path of 16 cm. In the range 400 – 6500 cm^{-1} the spectrum was recorded by a Bruker Vertex 70 spectrometer, with a resolution ranging from 1.0 up to 0.2 cm^{-1} and using a double walled, stainless steel cell (optical path of 13.4 cm), equipped with KBr windows. Cross section measurements (obtained at a resolution of 0.5 cm^{-1}) were carried out by keeping the cell temperature constant at 298(±0.5) K and by adding up to 256 interferograms to maximize the SNR. Distortions due to finite-resolution effects[68,69] were minimized, based on the methodologies established in precedent works,[70,71] by mixing the sample with N_2 (SIAD, purity > 99%) up to a total pressure of 101 kPa. Adsorption of the sample on the cell walls, checked by pressure monitoring and inspection of the absorption spectra, was found to be negligible over longer time than that needed to obtain a spectrum. 1-Bromo-1-fluoroethene was purchased from ABCR (with a stated purity > 97%) and used without any further purification.

2.2 Computational details and methodology.

To accurately characterize the molecular structure and the spectroscopic properties of 1-bromo-1-fluoroethylene, the equilibrium geometry and the harmonic force field were determined by means of a composite scheme that accounts simultaneously for basis-set and electron-correlation

effects. In particular, the so-called "cheap" geometry scheme[72–74] was employed. The starting point of this approach is the coupled-cluster model including single and double excitations with a perturbative treatment of triple excitations, CCSD(T),[75] within the frozen-core (fc) approximation in conjunction with the cc-pCVTZ(-PP) basis set.[76–78] The PP acronym above means that for bromine correlation-consistent basis sets were used together with small-core relativistic pseudopotentials, which leave 25 electrons to be handled explicitly. Actually, cc-pCVTZ(-PP) denotes that the cc-pCVTZ basis set was employed with the H, C and F atoms, while the cc-pVTZ(-PP) basis set was used for Br. To include the most relevant contributions in the electronic structure treatment, MP2 computations were carried out. In particular, the extrapolation to the complete basis set limit (CBS) was performed by means of the consolidated n^{-3} extrapolation formula:[79] this was applied to MP2 optimized geometries or harmonic force fields, obtained with triple- and quadruple-zeta quality basis sets (cc-pV*n*Z(-PP), *n* = T, Q). The contribution due to core-valence (CV) electron correlation was included by means of the corresponding correction, which is obtained from the comparison of MP2/cc-pCVTZ(-PP)[80] computations correlating all electrons with those performed within the fc approximation. The effect of diffuse functions in the basis set (aug), defined as difference between MP2/aug-cc-pVTZ(-PP)[78,81] and MP2/cc-pVTZ(-PP) calculations (within the fc approximation), was also taken into account. On the whole, our best estimate was determined as:

$$p(\mathrm{best}) = p(\mathrm{CCSD(T)/TZ}) + \Delta p(\mathrm{CBS}) + \Delta p(\mathrm{CV}) + \Delta p(\mathit{diff}) \quad (1)$$

where *p* denotes a generic structural parameter or harmonic force constant in a normal coordinate representation, with harmonic force fields being obtained using analytic second derivatives.[82] The reader is referred, for example, to Refs. 37 and 58 for a more detailed account and validation of the procedure. All these MP2 and CCSD(T) computations were carried out with the quantum-chemical program package CFOUR.[83]

For a semi-rigid rotor, the effect of molecular vibrations on the rotational parameters can be conveniently described by means of vibrational perturbation theory (VPT).[61–64] For the rotational constants of the *v*-th vibrational state, the vibrational dependency is expressed by an expansion in power of $(v + 1/2)$.[64] To the second-order (VPT2), only the linear term is needed. Therefore, for the vibrational ground state rotational constant with respect to the *i*-th inertial axis (with $i = a, b, c$, thus being, for example, $B^a = A$), the following expression is obtained:

$$B_0^i = B_e^i - \frac{d_r}{2}\sum_r \alpha_r^i \quad . \tag{2}$$

The sum in the right-hand side of Eq. (2) runs over all normal modes *r* and is defined as the vibrational correction, ΔB_{vib}; d_r is the degeneracy of the *r*-th vibrational mode, and α_r^i denotes the vibration–rotation interaction constant corresponding to the *r*-th mode and the *i*-th inertial axis. The equilibrium rotational constants, as depending only on the isotopic masses and the equilibrium geometrical parameters, were straightforwardly derived from the knowledge of the equilibrium structure.

Anharmonic corrections to rotational constants as well as vibrational energies and IR intensities required a VPT2[61–64] analysis applied to an anharmonic force field. This was obtained by numerical differentiation of displaced analytic hessians and first derivatives of the electric dipole moments along the normal coordinates at both MP2[60] and B2PLYP[59,84] levels of theory and employing the cc-pVTZ(-PP) basis set. Computations were carried out using the Gaussian suite of quantum chemical programs,[85] and a step of 0.01 $\sqrt{\text{u}}\cdot\text{bohr}$ in the numerical differentiation (where u is the unified atomic unit for mass, and bohr is the atomic unit for length).

By making use of the harmonic force fields evaluated in the frame of the composite scheme, best estimates for quartic centrifugal distortion constants were derived by means of an analogous composite scheme. The sextics[86] were evaluated from the cubic force fields mentioned above. Watson's *A*-reduced Hamiltonian in the I^r representation[87] was here considered. For the vibrational

energies and intensities of fundamental bands, overtones and combinations up to 3 quanta, hybrid models combining the harmonic frequencies from the composite scheme with the anharmonic force fields computed at the MP2 (HYB-1) and B2PLYP (HYB-2) levels have been used.

To overcome the problem of resonances impacting the VPT2 energies and intensities, two models were used, namely, the generalized VPT2 (GVPT2)[88] and hybrid degeneracy-corrected PT2 (HDCPT2), which differ mainly on the way the Fermi resonances (FRs) are handled to avoid unphysical results. In the former model, FRs are identified by means of a two-step procedure, which first assesses the difference of energy, $\Delta\omega$, between the potentially resonant harmonic states ($\Delta\omega^{1-2} \leq 200$ cm^{-1}) and then evaluates the deviation, K^{1-2}, of the VPT2 term from a model variational system involving those two steps, following the work of Martin and coworkers[89] ($K^{1-2} \geq 1$ cm^{-1}). Discarded terms are then treated variationally in a subsequent step. Details on the protocol can be found in Refs. [65, 88, 90]. The second model is derived from the work of Kuhler *et al.* (DCPT2),[91] where all potentially resonant terms in the definition of the vibrational energy are replaced by non-resonant forms derived from variational models. The hybrid variant (HDCPT2) introduces a mixing with the actual VPT2 results to compensate poorly suited transformations far from resonances (see Ref. 92 for details, the default parameters specified there for α and β have been used in this work). For both models, Darling-Dennison resonances (DDRs),[65,67,90] identified by a two-step procedure based on the energy difference between the harmonic states and the magnitude of the variational term ($\Delta\omega^{DD} \leq 100$ cm^{-1}, $K^{DD} \geq 10$ cm^{-1}),[66,93,94] were included through a variational step (for GVPT2, a single variational step is done).

3. RESULTS AND DISCUSSION

3.1. Equilibrium Geometry, Harmonic Force Field Data and Spectroscopic Parameters.

$BrFC=CH_2$ is a planar molecule belonging to the C_s point group, with its three principal axes of inertia illustrated in Figure 1. The molecule lies on the *ab* plane, while the *c* axis is perpendicular to the molecular plane. Therefore the A' vibrations will give rise to a/b-hybrid bands, while the A" modes will produce c-type band contours.

As addressed above, our computational investigation started with the accurate determination of the equilibrium geometry by means of the composite scheme described in the methodology section. This was the preliminary and mandatory step for the subsequent accurate determination of the harmonic force field by means of the same composite approach. As a byproduct of our computational study aimed at supporting and complementing the experimental analysis of the vibrational spectrum of $BrFC=CF_2$, all rotational spectroscopy parameters can be determined. Thanks to the available experimental data, this information can be used to check the accuracy of our results. Table 1 collects the equilibrium structural parameters at different levels of theory. More precisely, the results at the fc-CCSD(T)/cc-pCVTZ(-PP) level are reported together with the corrections of Eq. (1), i.e., CBS, CV and *diff*, as well as the overall best estimate. The corresponding equilibrium rotational constants and the various contributions to them are also reported in Table 1. We first of all note that, for most geometrical parameters, the fc-CCSD(T)/cc-pCVTZ(-PP) level of theory already provides accurate results, with the CBS and CV corrections ranging from 0.001 Å to 0.002 Å and the *diff* ones being smaller than 0.001 Å. The exceptions are the CBS corrections for the C=C and C-Br bond lengths that are -5 mÅ and -13 mÅ, respectively, and the *diff* corrections for the C-F and C-Br distances that are both 4 mÅ, but the former is positive (i.e., leads to a lengthening of the bond), while the latter is negative (shortening). It is also noted that the CBS and CV corrections to bond distances are negative, while the *diff* ones are generally positive, with the C-F bond being the only exception. Less systematic are the corrections for angles, which generally lie in the 0.1-0.3 degrees range. According to the literature on this topic,[37,58,72–74] the expected accuracy for the best-estimated bond distances is 0.001-0.002 Å, while that for angles is ~0.5 degrees. However, the structural parameters involving bromine are expected

to be affected by larger uncertainties,[95] with 0.003-0.004 Å providing a more reliable estimate for error bars.

Table 2 summarizes the rotational parameters (the ground state rotational constants and the quartic centrifugal distortion constants), while Table S1 in the Supplementary material lists the sextic centrifugal distortion constants for both ^{79}Br and ^{81}Br isotopologues. Analogously to Table 1, also in Table 2 we can point out how the various terms of Eq. (1) contribute to the best-estimated values. Concerning the rotational constants, the magnitude of the various contributions reflects the changing in the geometrical parameters discussed above. For quartic centrifugal distortion constants, the contributions are particularly small, in relative terms being smaller than 1%. More interesting is the comparison of our best-estimated values with experiment.[56] We note a good agreement: within 1% for rotational constants and in the 1–3 % range for centrifugal distortion constants. It is also interesting to note that our computations point out the limited accuracy of the experimental determination of Δ_K for both isotopic species. In fact, this constant should be very similar for the two isotopologues, while the experimental data differ by ~20%. In Ref. 56, the bromine quadrupole-coupling constants are also available. From a computational point of view, their determination requires the knowledge of the electric field gradient at the bromine nucleus. The corresponding calculation cannot be performed using a PP approach (as the one we employed), but it needs instead costly all-electron calculations, thus requiring relativistic effects to be explicitly considered.[96,97] Since such a determination is out of the scope of the present work, we did not further investigated the rotational spectroscopy properties.

Tables 3 and 4 summarize, for ^{79}BrFC=CH$_2$ and ^{81}BrFC=CH$_2$, respectively, the harmonic wavenumbers (ω_i) together with the corresponding IR intensities (km mol^{-1}) calculated within the double harmonic approximation. These tables are organized like Table 1: the fc-CCSD(T)/cc-pCVTZ(-PP) results are collected together with the CBS, CV and *diff* contributions and the overall best-estimated values. Concerning wavenumbers, it is interesting to note that, while CBS corrections can be either positive or negative, CV contributions are always positive and *diff*

corrections are always negative. The latter two contributions are of the same order of magnitude, with the *diff* ones being usually somewhat larger. As a consequence, they almost cancel out. Also the CBS corrections are of the same order of magnitude of the other two terms. Therefore, none of them can be neglected for a balanced description. Moving to IR intensities, we note that all three contributions can be either positive or negative (i.e., increasing or decreasing the intensities), are small and on the same order of magnitude. Therefore, we can assume that the IR intensities at the fc-CCSD(T)/cc-pCVTZ(-PP) level are already sufficiently accurate for supporting spectral analyses.

The analysis of each normal mode was then carried out on the basis of the total energy distribution (TED), as calculated by using the INTDER2005 program,[98] and employing the quadratic force constants, in a normal coordinate representation, at the CCSD(T)/cc-pCVTZ(-PP) level of theory. Starting from a set of internal coordinates, twelve symmetry-adapted internal coordinates (listed in Table 5) were defined in order to carry out the TED analysis. Referring to Figure 1 for the atom numbering, the bond length between the atoms *i* and *j* is denoted r_{ij}, and the angle enclosed by the bonds r_{ij} and r_{jk} (*j* being the apex atom) α_{ijk}. The symbol τ_{ijkl} represents the torsion angle between the planes formed by the atoms *ijk* and *jkl*, and the out-of-plane angle between the bond r_{ij} and the plane defined by the atoms *kjl* is denoted γ_{ijkl}. Based on the percentage of TED,[99] each fundamental vibration was therefore described in terms of the symmetry coordinates, and the results are listed in Table 6. As it can be seen, the CH_2 group vibrational modes (stretchings and bendings) are correctly described, with normal modes ω_1 and ω_2 associated to the asymmetric and symmetric stretchings, respectively, while ω_4 and ω_{10} are related to the scissor and wagging vibrations, their TED being dominated by the symmetry coordinates S_5 and S_{10}, respectively. Concerning normal modes ω_7 and ω_8, the TED analysis leads to the description of both of them as combinations of symmetric coordinates involving also the C-Br stretching; this is in agreement with the *ab initio* harmonic calculations that predict significant different values for these modes (the $^{79/81}$Br isotopologue splittings being larger than 0.5 cm^{-1}, see Tables 3 and 4). As found

also in other studies,[31,99,100] because of the inclusion of the off-diagonal interaction terms in the calculations of the TED (see expressions 30–32 of Ref. 99), for some normal modes the contribution due to a particular symmetry-adapted coordinate exceeds 100%.

3.2. Assignment of the Gas-Phase Infrared Spectra and Analysis of the Anharmonic Resonances.

We started the vibrational analysis by assigning the two lowest fundamentals in the 300 – 400 cm^{-1} region. Then, we proceeded to analyze the spectra recorded in the range 400 – 6500 cm^{-1}, starting from those obtained at lower pressure to assign first all the strongest fundamentals. The weakest ones were then identified in the spectra obtained at increasing pressure, which led also to the assignments of the remaining vibrational features in terms of overtone and combination bands (a survey spectrum of the 400 – 6500 cm^{-1} spectral region is illustrated in Figure 2). The cubic and semi-diagonal quartic force constants, as well as the anharmonicity constants obtained at both MP2 and B2PLYP levels of theory are collected in Tables S2-S7 of the Supplementary Material.

3.2.1. The ν_8 and ν_9 fundamentals. As it can be seen in Figure 3, both ν_8 (located at around 363 cm^{-1}) and ν_9 (located at 321.1 cm^{-1}) have almost the same intensity. The ν_8 band, which has a significant percentage of C-Br stretching (see Table 6), clearly shows the signals due to the presence of both the $^{79/81}$Br isotopologues, at 364.0 and 362.6 cm^{-1}, respectively; this observed splitting (1.4 cm^{-1}) is well predicted by the harmonic data (1.3 cm^{-1} at the CCSD(T)/cc-pCVTZ(-PP) level, 1.2 cm^{-1} according to the Best estimate prediction). Both hybrid models yield values in very good agreement with the experimental counterparts: for example, concerning ν_9, HYB-1 and HYB-2 predict this band at 325.2 cm^{-1} and 325.3 cm^{-1}, respectively. Moving to the ν_8 fundamental, the absorption due to the ^{79}Br isotopologue is calculated at 366.7 cm^{-1} by HYB-1, while the one related to the ^{81}Br isotopic species is predicted at 365.5 cm^{-1}.

3.2.2. The 400 – 700 cm^{-1} spectral region. This spectral region is characterized by the absorptions due to the ν_{12} (A") and ν_7 (A') fundamentals; the former is located at 476.1 cm^{-1}, while the latter (centered around 617 cm^{-1}) is almost an order of magnitude more intense. The observed splitting for ν_7 (around 0.5 cm^{-1}) due to the $^{79/81}$Br isotopologues is in good agreement with those calculated at both the harmonic (the best-estimated prediction is around 0.6 cm^{-1}) and anharmonic levels (both hybrid models yield a value around 0.7 cm^{-1}). In addition to these two fundamentals, absorptions due to hot bands from the $\nu_8 = 1$ and $\nu_9 = 1$ vibrational levels were identified and assigned, namely $\nu_9 + \nu_{12} - \nu_8$ and $\nu_{10} - \nu_9$.

3.2.3. The 700 – 1000 cm^{-1} spectral region. The intense absorptions due to ν_6 (centered at 946.4 cm^{-1}) and ν_{10} (centered at 839.0 cm^{-1}) dominate this spectral region, which also comprises the weak ν_{11} fundamental (located at 707.8 cm^{-1}) and other bands due to the $2\nu_8$ overtone (at 735.3 cm^{-1}), the $\nu_8 + \nu_{12}$ combination (the features due to $^{79/81}$Br isotopologues are clearly distinguishable at 840.7 and at 840.1 cm^{-1}, respectively), and the $2\nu_8 + \nu_{12} - \nu_9$ and $\nu_7 + 2\nu_9 - \nu_8$ hot bands (at 892.4 and at 895.8 cm^{-1}, respectively). According to both HYB-1 and HYB-2, the ν_6 fundamental is perturbed by a Fermi type 2 resonance with the nearby $\nu_7 + \nu_9$ combination band (overlapped by the stronger absorption features of ν_6) ; the diagonalization of the interaction matrix shifts the $\nu_6 = 1$ vibrational level down by about 3 cm^{-1}, thus leading to a predicted value of 939.8 cm^{-1} at the HYB-1 level (940.6 cm^{-1} according to HYB-2), in good agreement with the experimental data.

3.2.4. The 1000 – 1400 cm^{-1} spectral region. The main feature of this spectral region is the ν_5 band (at 1168.5 cm^{-1}), which is the most intense fundamental (169.9 km mol^{-1}); the other fundamental falling in this spectral region is ν_4 (at 1368.6 cm^{-1}), with an intensity almost two order of magnitude weaker than that of ν_5, and, according to both HYB-1 and HYB-2 force fields, perturbed by a Fermi type 2 interaction with the $\nu_{10} + \nu_{12}$ band. Their experimental positions and intensities are remarkably well predicted by both HYB-1 and HYB-2 hybrid force fields (agreement better than 3 cm^{-1} and 5% for position and intensity, respectively). Besides these two fundamentals,

this spectral region is characterized by the absorptions of some combination bands ($\nu_{11} + \nu_{12}$, $\nu_{10} + \nu_{12}$, $\nu_6 + \nu_8$, $\nu_7 + 2\nu_8$), the $2\nu_7$ overtone and some hot bands coming from the $\nu_8 = 1$ and $\nu_9 = 1$ vibrational levels.

3.2.5. The 1400 – 2000 cm^{-1} spectral region. The strong absorption due to ν_3 characterizes the spectrum in the range 1400 – 2000 cm^{-1}. According to both HYB-1 and HYB-2 force fields, this fundamental (located at 1647.3 cm^{-1}) is perturbed by a Fermi type 1 interaction with the first overtone of ν_{10} (see Figure 4). The HYB-1 force fields lead to calculated values for both ν_3 and $2\nu_{10}$ (obtained after diagonalization of the corresponding interaction matrix) in excellent agreement with the measured one (i.e. well within 1.0 cm^{-1}), while the HYB-2 predicted positions are, on average, about 8 cm^{-1} higher than the experimental data. In addition to these bands, we identified the absorptions due to many two-quanta combinations ($\nu_6 + \nu_{12}$, $\nu_5 + \nu_9$, $\nu_{10} + \nu_{11}$, $\nu_6 + \nu_7$, $\nu_4 + \nu_8$, $\nu_5 + \nu_7$, $\nu_5 + \nu_{11}$, $\nu_3 + \nu_9$, $\nu_4 + \nu_7$), and to the first overtone of ν_6 in this region of the spectrum. Both HYB-1 and HYB-2 hybrid force fields yield predicted values in more than good agreement with the measured ones (on average, the overall discrepancies are not greater than about 6 cm^{-1} and 2% for position and intensity, respectively).

3.2.6. The 2000 – 2900 cm^{-1} spectral region. In the spectral region between 2000 and 2900 cm^{-1} we identified weak features due to many two-quanta and some three-quanta combination bands, and the $2\nu_4$ overtone (at 2729.8 cm^{-1}). The predictions yielded by both hybrid force fields are in more than satisfactory agreement with the experimental data (discrepancies, on average, not greater than 10 cm^{-1} and 9% for position and intensity, respectively).

3.2.7. The 2900 – 3200 cm^{-1} spectral region. The ν_1 and ν_2 fundamentals characterize this spectral region. The latter (located at 3068.7 cm^{-1}) is perturbed by a Fermi type 2 resonance with $\nu_3 + \nu_4$; the diagonalization of the corresponding interaction matrix shifts up the fundamental by about 15 cm^{-1} thus leading to a calculated value in good agreement with the experimental one (HYB-1 and HYB-2 force fields predict this band at 3067.4 cm^{-1} and 3072.3 cm^{-1}, respectively). Besides these

two fundamentals, in the spectrum between 2900 and 3200 cm^{-1}, we identified the absorption features due to some two- and three-quanta combination bands.

3.2.8. The 3200 – 5900 cm^{-1} spectral region. This spectral region is characterized by the absorptions due to combination bands up to three-quanta and the first overtone of ν_3. On average, both HYB-1 and HYB-2 predictions are in good agreement with the measured data (on average, discrepancies smaller than 15 cm^{-1} and 15% for position and intensity, respectively).

3.2.9. The 5900 – 6500 cm^{-1} spectral region. The main features of this spectral region are the absorptions due to the first overtone of ν_1 and ν_2, located at 6260.4 and 6021.4 cm^{-1}, respectively. Between them we identified weaker features due to two- and three-quanta combination bands, namely $\nu_2 + \nu_3 + \nu_4$ (at 6061.2 cm^{-1}), $\nu_1 + \nu_2$ (at 6094.5 cm^{-1}) and $\nu_1 + \nu_3 + \nu_4$ (at 6147.5 cm^{-1}). On the basis of the thresholds employed here,[77] both HYB-1 and HYB-2 predict these vibrations essentially free from significant anharmonic resonances.

Table 7 lists all the assigned combination and overtone bands, while Table 8 reports the fundamentals along with their predicted values computed on the basis of the HYB-1 and HYB-2 force fields. Within the GVPT2 framework, both the hybrid force fields predict all fundamentals with good accuracy (the mean absolute deviation, MAD, of HYB-1 and HYB-2 being equal to 3.7 and 5.2 cm^{-1}, respectively). The same is observed for the HDCPT2 model, both hybrid force fields yield MAD of 4.2 and 4.8 cm^{-1} for HYB-1 and HYB-2, respectively. Considering the full set of assigned transitions, we can conclude that both HYB-1 and HYB-2 models and PT2 schemes are able to reproduce with more than satisfactory agreement the spectral range up to 6500 cm^{-1} (MAD not greater than 12 cm^{-1}), yielding accurate results also when dealing with rather relevant anharmonic interactions ($\nu_6/\nu_7 + \nu_9$, $\nu_4/\nu_{10} + \nu_{12}$, $\nu_3/2\nu_{10}$, $\nu_2/\nu_3 + \nu_4$).

3.3. Absorption Cross Sections, Integrated Band Intensities, and Comparison with the Calculated Anharmonic Dipole Moment Surface.

In order to determine the absorption cross section spectra, we recorded several spectra at increasing sample pressures, and using N_2 as inert buffer gas (as detailed in the Experimental details section). Following a consolidated procedure established in previous studies,[31,36,70] we carried out the analysis by least-squares fitting the point-by-point absorbance value $A(\tilde{\nu})$, measured at each wavenumber, $\tilde{\nu}$, versus the corresponding sample concentration. The slope thus computed at each wavenumber, $\sigma(\tilde{\nu})$, yields the absorbance cross section per molecule (cm^2 $molecule^{-1}$):

$$\sigma(\tilde{\nu}) = \frac{A(\tilde{\nu})\ln(10)}{N_A c l} \quad (3)$$

where N_A is the Avogadro's constant, c is the sample concentration (mol cm^{-3}) and l represents the optical path length (cm); the statistical uncertainty at each wavenumber, associated to the slope computed by the fitting procedure, represents the corresponding error. The absorption cross-section spectrum thus derived (in the region 400 – 6500 cm^{-1}) is reported in Figure 5; as it can be seen, the intense features due to the strong ν_3 and ν_5 fundamentals clearly dominate over all the other absorptions. The region between 400 and 1000 cm^{-1} is characterized by the ν_{10}, ν_7 and ν_6 fundamentals, having intensities ranging from about 30 to almost 50 km mol^{-1}, while ν_1 and ν_2 (in the 2900 – 3200 cm^{-1} spectral region) are significantly weaker (less than 1 and 4 km mol^{-1}, respectively). Moving to higher wavenumber, the most relevant absorption features characterizing the spectrum in the range 4000 – 5000 cm^{-1} are due to two-quanta combination bands, while the first overtones of ν_1 and ν_2 dominate the 5900 – 6300 cm^{-1} region. Table 9 lists the integrated band intensities determined from the analysis of the absorption cross-section spectrum together with the corresponding computed GVPT2 data obtained from both HYB-1 and HYB-2 hybrid force fields. As it can be seen, they are able to accurately reproduce the experimental data, their errors on the most intense features being on average not greater than 7%. Considering the whole data set up to

6500 cm^{-1}, the MAD is less than 0.9 km mol^{-1} for both HYB-1 and HYB-2, thus highlighting the overall reliability of the calculated anharmonic dipole moment surface.

4. CONCLUSIONS

High-level quantum-chemical predictions of spectroscopic parameters of 1-bromo-1-fluoroethene are required to support and guide future high-resolution studies on this molecule. The composite scheme employed in the present work (accounting for extrapolation to the infinite basis-set limit and electron correlation effects) provided accurate equilibrium geometry and harmonic force field. These data, together with the anharmonic corrections (obtained at both the MP2 and B2PLYP level of theory) yielded reliable values for the spectroscopic parameters relevant to rotational spectroscopy (ground state rotational constants, quartic and sextic centrifugal distortion constants, etc.) for both $^{79}BrFC=CH_2$ and $^{81}BrFC=CH_2$, also pointing out the limited accuracy of the experimental value of Δ_K reported in the literature. On the basis of the spectra recorded at medium resolution, we assigned the whole vibrational structure up to 6500 cm^{-1} in terms of fundamentals, overtones and combinations (up to three-quanta). Even if several bands turned out to be affected by anharmonic interactions, their predictions obtained within the framework of VPT2 theory were found in good agreement with the experimental data. From the computed dipole moment surface, the IR integrated band intensities were predicted and compared to the accurate values obtained from the measured absorption cross section spectra. The overall excellent agreement between experimental and predicted data (both transition wavenumbers and intensities) confirms the accuracy and reliability of the present investigation.

Supporting Information

The Supporting Information is available free of charge on the ACS Publications website at DOI:

Tables S1–S7 listing the computed sextic centrifugal distortion constants, the cubic and semi-diagonal quartic force constants, and the anharmonicity constants obtained at both the MP2 and B2PLYP levels of theory in conjunction with the cc-pVTZ(-PP) basis set.

ACKNOWLEDGEMENTS

This work has been supported by MIUR (PRIN 2012 funds for project "STAR: Spectroscopic and computational Techniques for Astrophysical and atmospheric Research", prot. no. 20129ZFHFE_003), by University Ca' Foscari Venezia (ADIR funds), by University of Bologna (RFO funds), and by National Natural Science Foundation of China (Grant No. 91641128). The High Performance Computing department of the CINECA Supercomputer Centre (Grant No. HP10C292PO), the SCSCF ("*Sistema per il Calcolo Scientifico di Ca' Foscari*") facility, and the SMART@SNS Laboratory (http://dreams.sns.it) are gratefully acknowledged for the utilization of computer resources. The support of the COST CMTS-Actions CM1405 (MOLIM: MOLecules In Motion) and CM1401 (Our Astro-Chemical History) is also acknowledged.

REFERENCES

(1) Huang B.; Lei, C.; Wei, C.; Zeng, G. Chlorinated Volatile Organic Compounds (Cl-VOCs) in Environment - Sources, Potential Human Health Impacts, and Current Remediation Technologies. *Environ. Int.* **2014**, *71*, 118–138.

(2) Dobrzyńska, E.; Pośniak, M.; Szewczyńska, M.; Buszewski, B. Chlorinated Volatile Organic Compounds—Old, However, Actual Analytical and Toxicological Problem. *Crit. Reviews in Anal. Chemistry*, **2010**, *40*, 41–57.

(3) Mattes, E. T.; Alexander, A. K.; Coleman, N. V. Aerobic Biodegradation of the Chloroethenes: Pathways, Enzymes, Ecology, and Evolution. *Microb. Reviews* **2010**, *34*, 445–475.

(4) *IARC Monographs on the Evaluation of Carcinogenic Risks to Humans*, Vol. 97; International Agency for Research on Cancer; Lyon, **2008**, and references therein.

(5) Hossaini, R.; Chipperfield, M. P.; Montzka, S. A.; Rap, A.; Dhomse, S.; Feng, W. Efficiency of Short-lived Halogens at Influencing Climate through Depletion of Stratospheric Ozone. *Nat. Geoscience* **2015**, *8*, 186–190.

(6) Simpson, W. R.; Brown, S. S.; Saiz-Lopez, A.; Thornton, J. A.; von Glasow, R. Tropospheric Halogen Chemistry: Sources, Cycling, and Impacts. *Chem. Rev.* **2015**, *115*, 4035–4062.

(7) Saiz-Lopez, A.; von Glasow, R. Reactive Halogen Chemistry in the Troposphere. *Chem. Soc. Rev.* **2012**, *41*, 6448 –6472.

(8) Dessens, O.; Zeng, G.; Warwick, N.; Pyle, J. Short-lived Bromine Compounds in the Lower Stratosphere; Impact of Climate Change on Ozone. *Atmos. Sci. Lett.* **2009**, *10*, 201–206.

(9) von Glasow, R.; von Kuhlmann, R.; Lawrence, M. G.; Platt, U.; Crutzen, P. J. Impact of Reactive Bromine Chemistry in the Troposphere. *Atmos. Chem. Phys.* **2004**, *4*, 2481–2497.

(10) McNaughton, D.; Robertson, E. G.; Thompson, C. D.; Chimdi, T.; Bane, M. K. Appadoo, D. Overview of High-Resolution Infrared Measurement and Analysis for Atmospheric Monitoring of Halocarbons. *Anal. Chem.* **2010**, *82*, 7958–7964.

(11) Canè, E.; Villa, M.; Tamassia, F.; Pietropolli Charmet, A.; Tasinato, N.; Stoppa, P.; Giorgianni, S. The Ro-Vibrational Analysis of the ν_4 Fundamental Band of CF_3Br from Jet-Cooled Diode Laser and FTIR Spectra in the 8.3μm Region. *Mol. Phys.* **2014**, *112*, 1899–1909.

(12) Brumfield, B. E.; Stewart, J. T.; Widicus Weaver, S. L.; Escarra, M. D.; Howard, S. S.; Gmachl, C. F.; McCall, B. J. A Quantum Cascade Laser Cw Cavity Ringdown Spectrometer Coupled to a Supersonic Expansion Source. *Rev. Sci. Instrum.* **2010**, *81*, 063102.

(13) di Lauro, C.; D'Amico, G.; Snels, M. Torsional Splittings in the Diode Laser Slit-Jet Spectra of the ν_6 Fundamental of 1-Chloro-1,1-Difluoroethane (HCFC-142b). *J. Mol. Spectrosc.* **2009**, *254*, 108–118.

(14) Pietropolli Charmet, A.; Stoppa, P.; Toninello, P.; Baldacci, A.; Giorgianni, S. Jet-Cooled Diode Laser Spectra of CF_3Br in the 9.2 μm Region and Rovibrational Analysis of Symmetric CF_3 Stretching Mode. *Phys. Chem. Chem. Phys.* **2006**, *8*, 2491–2498.

(15) Herman, M.; Georges, R.; Hepp, M.; Hurtmans, D. High Resolution Fourier Transform Spectroscopy of Jet-Cooled Molecules. *Int. Rev. Phys. Chem.* **2000**, *19*, 277–325.

(16) Wugt Larsen, R.; Hegelund, F.; Engdahl, A.; Uvdal, P.; Nelander, B. High-Resolution Infrared Study of Collisionally Cooled trans-1,2-Dichloroethylene. *J. Mol. Spectrosc.* **2007**, *243*, 99–102.

(17) Albert, S.; Baurecker, S.; Quack, M.; Steinlin, A. Rovibrational Analysis of the $2\nu_3$, $3\nu_3$ and ν_1 Bands of $CHCl_2F$ Measured at 170 and 298 K by High-Resolution FTIR Spectroscopy. *Mol. Phys.* **2007**, *105*, 541–558.

(18) Thompson, C. D.; Robertson, E. G.; McNaughton, D. Completing the Picture in the Rovibrational Analysis of Chlorodifluoromethane ($CHClF_2$): ν_3 and ν_8. *Mol. Phys.* **2004**, *102*, 1987–1695.

(19) Bauerecker, S.; Taraschewski, M.; Weitkamp, C.; Cammenga, H. K. Liquid-helium Temperature Long-Path Infrared Spectroscopy of Molecular Clusters and Supercooled Molecules. *Rev. Sci. Instrum.* **2001**, *72*, 3946–3955.

(20) Almeida, M. M.; Prudente, F. V.; Fellows, C. E.; Marques, J. M. C.; Pereira, F. B. Direct Fit of Spectroscopic Data of Diatomic Molecules by Using Genetic Algorithms: II. The Ground State of RbCs. *J. Phys. B: At. Mol. Opt. Phys.* **2011**, *44*, 225102.

(21) Marques, J. M. C.; Prudente, F. V.; Pereira, F. B.; Almeida, M. M.; Maniero, A. M.; Fellows, C. E. A New Genetic Algorithm to be Used in the Direct Fit of Potential Energy Curves to Ab Initio and Spectroscopic Data. *J. Phys. B: At. Mol. Opt. Phys.* **2008**, *41*, 085103.

(22) Lees, R. M.; Li, L.; Xu, Li-H. New VISTA on Ammonia in the 1.5 μm Region: Assignments for the $\nu_3 + 2\nu_4$ Bands of $^{14}NH_3$ and $^{15}NH_3$ by Isotopic Shift Labeling. *J. Mol. Spectrosc.* **2008**, *251*, 241–251.

(23) Lodyga, W.; Kreglewski, M.; Pracna, P.; Urban, S. Advanced Graphical Software for Assignments of Transitions in Rovibrational Spectra. *J. Mol. Spectrosc.* **2007**, *243*, 182–188.

(24) Tasinato, N.; Pietropolli Charmet, A.; Stoppa, P. ATIRS package: A Program Suite for the Rovibrational Analysis of Infrared Spectra of Asymmetric Top Molecules. *J. Mol. Spectrosc.* **2007**, *243*, 148–154.

(25) Robertson, E.G.; McNaughton, D. Maximising Rovibrational Assignments in the ν_1 Band of NSCl by Spectral Analysis by Subtraction of Simulated Intensities (SASSI). *J. Mol. Spectrosc.* **2006**, *238*, 56–63.

(26) Meerts, W. L.; Schmitt, M. A New Automated Assign and Analysing Method for High-Resolution Rotationally Resolved Spectra Using Genetic Algorithms. *Phys. Scripta* **2005**, *73*, C47-C52.

(27) Medvedev, I. R.; Winnewisser, M.; Winnewisser, B. P.; De Lucia, F. C.; Herbst, E. The Use of CAAARS (Computer Aided Assignment of Asymmetric Rotor Spectra) in the Analysis of Rotational Spectra. *J. Mol. Struct.* **2005**, *742*, 229–236.

(28) Császár, A. G.; Fábri, C.; Szidarovszky, T.; Mátyus, E.; Furtenbachera, T.; Czakó, G. The Fourth Age of Quantum Chemistry: Molecules in Motion. *Phys. Chem. Chem. Phys.* **2012**, *14*, 1085–1106.

(29) Pesonen, J.; Halonen, L. *Recent Advances in the Theory of Vibration-Rotation Hamiltonians;* in *Advances in Chemical Physics, Vol. 125;* Ed. Prigogine, I. and Rice, S. A. John Wiley & Sons, Hoboken (USA), 2003.

(30) Carter, S.; Sharma, A. R.; Bowman, J. M.; Rosmus, P.; Tarroni, R. Calculations of Rovibrational Energies and Dipole Transition Intensities for Polyatomic Molecules Using MULTIMODE. *J. Chem. Phys.* **2009**, *131* 224106.

(31) Pietropolli Charmet, A.; Stoppa, P.; Tasinato, N.; Giorgianni, S.; Gambi, A. Study of the Vibrational Spectra and Absorption Cross Sections of 1-Chloro-1-fluoroethene by a Joint Experimental and *Ab Initio* Approach. *J. Phys. Chem. A* **2016**, *120*, 8369–8386.

(32) Medcraft, C.; Fuss, W.; Appadoo, D. R. T.; McNaughton, D.; Thompson, C. D.; Robertson, E. G. Structural, Vibrational, and Rovibrational Analysis of Tetrafluoroethylene. *J. Chem. Phys.* **2012**, *137*, 214301.

(33) Tasinato, N.; Pietropolli Charmet, A.; Stoppa, P.; Giorgianni, S.; Gambi, A. Quantum-Chemical *Ab Initio* Investigation of the Vibrational Spectrum of Halon 1113 and its Anharmonic Force Field: a Joint Experimental and Computational Approach. *Chem. Phys.* **2012**, *397*, 55−64.

(34) McKean, D.; Law, M. M.; Groner, P.; Conrad, A. R.; Tubergen, M. J.; Feller, D.; Moore, M. C.; Craig, N. C. Infrared Spectra of CF_2=CHD and CF_2=CD_2: Scaled Quantum-Chemical Force Fields and an Equilibrium Structure for 1,1-Difluoroethylene. *J. Phys. Chem. A* **2010**, *114*, 9309–9318.

(35) Carnimeo, I.; Puzzarini, C.; Tasinato, N.; Stoppa, P.; Pietropolli Charmet, A.; Biczysko, M.; Cappelli, C.; Barone, V. Anharmonic Theoretical Simulations of Infrared Spectra of Halogenated Organic Compounds. *J. Chem. Phys.* **2013**, *139*, 074310.

(36) Pietropolli Charmet, A.; Stoppa, P.; Tasinato, N.; Giorgianni, S; Barone, V.; Biczysko, M. Bloino, J.; Cappelli, C.; Carnimeo, I.; Puzzarini, C. An Integrated Experimental and Quantum-Chemical Investigation on the Vibrational Spectra of Chlorofluoromethane. *J. Chem. Phys.* **2013**, *139*, 164302.

(37) Barone, V.; Biczysko, M.; Bloino, J.; Puzzarini, C. Accurate Molecular Structures and Infrared Spectra of trans-2,3-Dideuterooxirane, Methyloxirane, and trans-2,3-Dimethyloxirane. *J. Chem. Phys.* **2014**, *141*, 034107.

(38) Biczysko, M.; Tarroni, R. Renner-Teller Interactions Coupled to Large Spin-orbit Splittings: The $BrCN^+$ Case. *Chem. Phys. Lett.* **2005**, *415*, 223–229.

(39) Tasinato, N.; Regini, G.; Stoppa, P.; Pietropolli Charmet, A.; Gambi, A. Anharmonic Force Field and Vibrational Dynamics of CH_2F_2 up to 5000 cm^{-1} Studied by Fourier Transform Infrared Spectroscopy and State-of-the-Art *Ab Initio* Calculations. *J. Chem. Phys.* **2012**, *136*, 214302.

(40) Pietropolli Charmet, A.; Tasinato, N.; Stoppa, P.; Giorgianni, S.; Gambi, A. Anharmonic Resonances in the CH Chromophore Overtone Spectra of $CHBrF_2$. *Mol. Phys.* **2011**, *109*, 2163-2172.

(41) Piccardo, M.; Penocchio, E.; Puzzarini, C.; Biczysko, M.; Barone, V. Semi-Experimental Equilibrium Structure determinations by Employing B3LYP/SNSD Anharmonic Force

Fields: Validation and Application to Semirigid Organic Molecules. *J. Phys. Chem. A* **2015**, *119*, 2058–2082.

(42) Feller, D.; Craig, N. C.; Groner, P.; McKean, D. C. *Ab Initio* Coupled Cluster Determination of the Equilibrium Structures of *cis*- and *trans*-1,2-Difluoroethylene and 1,1-Difluoroethylene. *J. Phys. Chem. A* **2011**, *115*, 94–98.

(43) Feller, D.; Peterson, K. A.; Dixon, D. A. *Ab Initio* Coupled Cluster Determination of the Heats of Formation of $C_2H_2F_2$, C_2F_2, and C_2F_4. *J. Phys. Chem. A* **2011**, *115*, 1440–1451.

(44) Banerjee, D.; Ghosh, A.; Chattopadhyay, S.; Ghosh, P.; Chaudhuri, R. K. Revisiting the 'cis-effect' in 1,2-Difluoro Derivatives of Ethylene and Diazene Using *Ab Initio* Multireference Methods. *Mol. Phys.* **2014**, *112*, 3206–3224.

(45) Jenkins, S.; Kirk, S. R.; Rong, C.; Yin, D. The Cis-effect Using the Topology of the Electronic Charge Density. *Mol. Phys.* **2013**, *111*, 793–805.

(46) Pietropolli Charmet, A.; Stoppa, P.; Tasinato, N.; Giorgianni. S. Computing Sextic Centrifugal Distortion Constants by DFT: a Benchmark Analysis on Halogenated Compounds. *J. Mol. Spectrosc.* **In press**, DOI:10.1016/j.jms.2017.02.006.

(47) Krasnoshchekov, S. V.; Craig, N. C.; Stepanov, N.F. Anharmonic Vibrational Analysis of the Gas-Phase Infrared Spectrum of 1,1-Difluoroethylene Using the Operator Van Vleck Canonical Perturbation Theory. *J. Phys. Chem. A* **2013**, *117*, 3041–3056.

(48) Tasinato, N.; Stoppa, P.; Pietropolli Charmet, A.; Giorgianni, S.; Gambi, A. Modelling the Anharmonic and Coriolis Resonances Within the Six Level Polyad Involving the ν_4 Fundamental in the Ro-vibrational Spectrum of Vinyl Fluoride. *J. Quant. Spectrosc. Radiat. Transfer* **2012**, *113*, 1240–1249.

(49) McKean, D. C.; van der Veken, B.; Herrebout, W.; Law, M. M.; Brenner, M. J.; Nemchick, D. J.; Craig, N. C. Infrared Spectra of $^{12}CF_2{}^{12}CH_2$ and $^{12}CF_2{}^{13}CH_2$, Quantum-Chemical Calculations of Anharmonicity, and Analyses of Resonances. *J. Phys. Chem. A* **2010**, *114*, 5728−5742.

(50) Tasinato, N.; Stoppa, P.; Pietropolli Charmet, A.; Giorgianni, S.; Gambi, A. High-resolution Infrared Study of Vinyl Fluoride in the 750 – 1050 cm^{-1} Regions: Rovibrational Analysis and Resonances Involving the ν_8, ν_{10} and ν_{11} Fundamentals. *J. Phys. Chem. A* **2006**, *110*, 13412–13418.

(51) Stoppa, P.; Pietropolli Charmet, A.; Tasinato, N.; Giorgianni, S.; Gambi, A. Infrared Spectra, Integrated Band Intensities, and Anharmonic Force Field of H_2C=CHF. *J. Phys. Chem. A* **2009**, *113*, 1497–1504.

(52) Tasinato, N.; Moro, D.; Stoppa, P.; Pietropolli Charmet, A.; Toninello, P.; Giorgianni, S. Adsorption of F_2C=CFCl on TiO2 Nano-Powder: Structures, Energetics and Vibrational Properties from DRIFT Spectroscopy and Periodic Quantum Chemical Calculations. *Appl. Surf. Sci.* **2015**, *353*, 986–994.

(53) Scaranto, J.; Mallia, G.; Harrison, N. M. An Efficient Method for Computing the Binding Energy of an Adsorbed Molecule Within a Periodic Approach. The Application to Vinyl Fluoride at Rutile TiO_2 (1 1 0) Surface. *Comput. Mat. Science* **2011**, *50*, 2080–2086.

(54) Scaranto, J.; Pietropolli Charmet, A.; Giorgianni, S. IR Spectroscopy and Quantum-Mechanical Studies of the Adsorption of CH_2CClF on TiO_2. *J. Phys. Chem. C* **2008**, *112*, 9443−9447.

(55) Scaranto, J.; Pietropolli Charmet, A.; Stoppa, P.; Giorgianni, S. Vinyl Halides Adsorbed on TiO2 Surface: FTIR Spectroscopy Studies and *Ab Initio* Calculations. *J. Mol. Struct.* **2005**, *741*, 213–219.

(56) Shimada, J.; Tatamitani, Y.; Liu, B.; Ogata, T. Microwave Spectra, Structures, and Nuclear Quadrupole Coupling Constants of Bromofluoroethenes: $BrFC=CH_2$, *cis*-BrHC=CHF and *trans*-BrHC=CHF. *J. Mol. Struct.* **2002**, *612*, 155–166.

(57) Scaranto, J.; Stoppa, P.; Pietropolli Charmet, A.; Giorgianni, S. IR Spectroscopy of CH_2CBrF Adsorbed on TiO_2 and Quantum-Mechanical Studies. *Mol. Phys.* **2009**, *107*, 237–244.

(58) Barone, V.; Biczysko, M.; Bloino, J.; Puzzarini, C. Accurate Structure, Thermodynamic and Spectroscopic Parameters from CC and CC/DFT Schemes: the Challenge of the Conformational Equilibrium in Glycine. *Phys. Chem. Chem. Phys.* **2013**, *15*, 10094–101110.

(59) Grimme, S. Semiempirical Hybrid Density Functional with Perturbative Second-order Correlation. *J. Chem. Phys.* **2006**, *124*, 034108.

(60) Møller, C; Plesset, M. S. Note on an Approximation Treatment for Many-Electron Systems. *Phys. Rev.* **1934**, *46*, 618–622.

(61) Nielsen, H. H. The Vibration-Rotation Energies of Molecules. *Rev. Mod. Phys.* **1951**, *23*, 90–136.

(62) Amat, G.; Nielsen, H.H.; Tarrago, G. *Rotation-Vibration of Polyatomic Molecules*: Marcel Decker: Amsterdam, 1971.

(63) Papoušek, D.; Aliev, M. R. *Molecular Vibrational-Rotational Spectra*; Elsevier: Amsterdam, 1982.

(64) Mills, I. M. in *Molecular Spectroscopy: Modern Research*; Ed. Rao, K. N.; Mathews, C.W. Academic: New York, 1972.

(65) Bloino, J.; Barone, V.A Second-Order Perturbation Theory Route to Vibrational Averages and Transition Properties of Molecules: General Formulation and Application to Infrared and Vibrational Circular Dichroism Spectroscopies. *J. Chem. Phys.* **2012**, *136*, 124108.

(66) Bloino, J. A VPT2 Route to Near-Infrared Spectroscopy: The Role of Mechanical and Electrical Anharmonicity. *J. Phys. Chem. A* **2015**, *119*, 5269–5287.

(67) Bloino, J.; Biczysko, M.; Barone, V. Anharmonic Effects on Vibrational Spectra Intensities: Infrared, Raman, Vibrational Circular Dichroism and Raman Optical Activity. *J. Phys. Chem. A* **2015**, *119*, 11862–11874.

(68) Ahro, M.; Kauppinen, J. Nonlinearity of Beer's Law in Gas-Phase FT-IR Spectroscopy. *Appl. Spectrosc.* **2001**, *55*, 50−54.

(69) Parker, F. ; Tooke, P. B. The Effect of Apodisation and Finite Resolution on Fourier Transform Infrared and Raman Spectra. *Spectrochim. Acta A* **1997**, *53*, 2245−2252.

(70) Pietropolli Charmet, A.; Stoppa, P.; Tasinato, N.; Baldan, A.; Giorgianni, S.; Gambi, A. Spectroscopic Study of $CHBrF_2$ up to 9500 cm^{-1}: Vibrational Analysis, Integrated Band Intensities, and *Ab Initio* Calculations. *J. Chem. Phys.* **2010**, *133*, 044310.

(71) Pietropolli Charmet, A.; Tasinato, N.; Stoppa, P.; Baldacci, A.; Giorgianni, S. Jet-Cooled Diode Laser Spectrum and FTIR Integrated Band Intensities of CF_3Br: Rovibrational Analysis of $2\nu_5$ and $\nu_2+\nu_3$ Bands Near 9 μm and Cross-Section Measurements in the 450–2500 cm^{-1} Region. *Mol. Phys.* **2008**, *106*, 1171−1179.

(72) Puzzarini, C.; Barone, V. Extending the Molecular Size in Accurate Quantum-Chemical Calculations: the Equilibrium Structure and Spectroscopic Properties of Uracil. *Phys. Chem. Chem. Phys.* **2011**, *13*, 7158−7166.

(73) Puzzarini, C.; Biczysko, M.; Barone, V.; Peña, I.; Cabezas, C.; Alonso, J. L. Accurate Molecular Structure and Spectroscopic Properties of Nucleobases: a Combined Computational–Microwave Investigation of 2-Thiouracil as a Case Study. *Phys. Chem. Chem. Phys.* **2013**, *15*, 16965−16975.

(74) Puzzarini, C.; Biczysko, M.; Barone, V.; Largo, L.; Peña, I.; Cabezas, C.; Alonso, J. L. Accurate Characterization of the Peptide Linkage in the Gas Phase: A Joint Quantum-Chemical and Rotational Spectroscopy Study of the Glycine Dipeptide Analogue. *J. Phys. Chem. Lett.* **2014**, *5*, 534−540.

(75) Raghavachari, K.; Trucks, G. W.; Pople, J. A.; Head-Gordon, M. A Fifth-Order Perturbation Comparison of Electron Correlation Theories. *Chem. Phys. Lett.* **1989**, *157*, 479–483.

(76) Dunning, T. H., Jr. Gaussian Basis Sets for Use in Correlated Molecular Calculations. I. The Atoms Boron through Neon and Hydrogen. *J. Chem. Phys.* **1989**, *90*, 1007–1023.

(77) Woon, D. E.; Dunning, T. H., Jr. Gaussian Basis Sets for Use in Correlated Molecular Calculations. V. Core-Valence Basis Sets for Boron through Neon. *J. Chem. Phys.* **1995**,

103, 4572–4585.

(78) Peterson, K. A.; Figgen, D.; Goll, E.; Stoll, H.; Dolg, M. Systematically Convergent Basis Sets with Relativistic Pseudopotentials. II. Small-core Pseudopotentials and Correlation Consistent Basis Sets for the Post-d Group 16–18 Elements. *J. Chem. Phys.* **2003**, 119, 11113.

(79) Helgaker, T.; Klopper, W.; Koch, H.; Noga, J. Basis-Set Convergence of Correlated Calculations on Water. *J. Chem. Phys.* **1997**, *106*, 9639−9646.

(80) Peterson, K. A.; Yousaf, K. E. Molecular Core-Valence Correlation Effects Involving the Post-d Elements Ga - Rn: Benchmarks and New Pseudopotential-Based Correlation Consistent Basis Sets. *J. Chem. Phys.* **2010**, *133*, 174116.

(81) Kendall, R. A.; Dunning, T. H., Jr.; Harrison, R. J. Electron Affinities of the First-row Atoms Revisited. Systematic Basis Sets and Wave Functions. *J. Chem. Phys.* **1992**, *96*, 6796−6806.

(82) Stanton, J. F.; Gauss, J. Analytic Second Derivatives in High-Order Many-Body Perturbation and Coupled-Cluster Theories: Computational Considerations and Applications. *Int. Rev. Phys. Chem.* **2000**, *19*, 61−95.

(83) CFOUR, Coupled-Cluster techniques for Computational Chemistry, a quantum-chemical program package by Stanton, J. F.; Gauss, J. ; Harding, M. E. *et al.*, and the integral packages MOLECULE (Almlöf, J.; Taylor, P. R.), PROPS (Taylor, P. R.), ABACUS (Helgaker, T.; Jensen, H. J. Aa. ; Jørgensen, P. and Olsen, J.), and ECP routines by Mitin, A. V., and Wüllen, C. For the current version, see http://www.cfour.de.

(84) Biczysko, M.; Panek, P.; Scalmani, G.; Bloino, J.; Barone, V. Harmonic and Anharmonic Vibrational Frequency Calculations with the Double-Hybrid B2PLYP Method: Analytic Second Derivatives and Benchmark Studies. *J. Chem. Theory Comput.* **2010**, 6, 2115−2125.

(85) Frisch, M. J.; Trucks, G. W.; Schlegel, H. B.; Scuseria, G. E.; Robb, M. A.; Cheeseman, J. R.; Scalmani, G.; Barone, V.; Petersson, G. A.; Nakatsuji, H., Li, X., et al., *Gaussian 2016*, Revision A.03, Gaussian, Inc., Wallingford, CT, 2016.

(86) Puzzarini, C.; Cazzoli, G.; Gauss, J. The Rotational Spectra of $HD^{17}O$ and $D_2{}^{17}O$: Experiment and Quantum-Chemical Calculations. *J. Chem. Phys.* **2012**, *137*, 154311.

(87) Watson, J. K. G. In *Vibrational Spectra and Structure*, Ed. Durig, J. R. Elsevier: New York, 1977, vol. 6, pp. 1–89.

(88) Piccardo, M; Bloino, J.; Barone, V. Generalized Vibrational Perturbation Theory for Rotovibrational Energies of Linear, Symmetric and Asymmetric Tops: Theory, Approximations, and Automated Approaches to Deal with Medium-to-Large Molecular Systems. *Int. J. Quantum Chem.* **2015**, *115*, 948–982.

(89) Martin, J. M. L.; Lee, T. J.; Taylor, P. M.; François, J.-P. The Anharmonic Force Field of Ethylene, C_2H_4, by Means of Accurate Ab Initio Calculations. *J. Chem. Phys.* **1995**, *103*, 2589–2602.

(90) Bloino, J.; Baiardi, A.; Biczysko, M. Aiming at an Accurate Prediction of Vibrational and Electronic Spectra for Medium-to-large Molecules: An Overview. *Int. J. Quant. Chem.* **2016**, *116*, 1543–1574 .

(91) Kuhler, K. M.; Truhlar, D. G.; Isaacson, A. D. General Method for Removing Resonance Singularities in Quantum Mechanical Perturbation Theory. *J. Chem. Phys.* **1996**, *104*, 4664–4670.

(92) Bloino, J.; Biczysko, M.; Barone, V. General Perturbative Approach for Spectroscopy, Thermodynamics, and Kinetics: Methodological Background and Benchmark Studies. *J. Chem. Theory Comput.* **2012**, *8*, 1015–1036.

(93) Rosnik, A. M.; Polik, W. F. VPT2+K Spectroscopic Constants and Matrix Elements of the Transformed Vibrational Hamiltonian of a Polyatomic Molecule with Resonances Using Van Vleck Perturbation Theory. *Mol. Phys.* **2014**, *112*, 261–300.

(94) Krasnoshchekov, S. V.; Isayeva, E. V.; Stepanov, N. F. Criteria for First- and Second-order Vibrational Resonances and Correct Evaluation of the Darling-Dennison Resonance Coefficients Using the Canonical Van Vleck Perturbation Theory. *J. Chem. Phys.* **2014**, *141*, 234114.

(95) Puzzarini, C.; Cazzoli, G.; Baldacci, A.; Baldan, A.; Michauk, C.; Gauss, J. Rotational Spectra of Rare Isotopic Species of Bromofluoromethane: Determination of the Equilibrium Structure from *Ab Initio* Calculations and Microwave Spectroscopy. *J. Chem. Phys.* **2007**, *127*, 164302.

(96) Puzzarini, C.; Stanton, J. F.; Gauss, J. Quantum-Chemical Calculation of Spectroscopic Parameters for Rotational Spectroscopy. *Int. Rev. Phys. Chem.* **2010**, *29*, 273–367.

(97) Puzzarini, C.; Cazzoli, G.; López, J. C.; Alonso, J. L., Baldacci, A.; Baldan, A.; Stopkowicz, S.; Cheng, L.; Gauss, J. Spectroscopic Investigation of Fluoroiodomethane, CH_2FI: Fourier-Transform Microwave and Millimeter-/Submillimeter-Wave Spectroscopy and Quantum-Chemical Calculations. *J. Chem. Phys.* **2011**, *134*, 174312.

(98) INTDER2005 is a general program developed by Wesley D. Allen and co-workers which performs various vibrational analyses and higher-order nonlinear transformations among force field representations.

(99) Allen, W. D.; Császár, A. G.; Horner, D. A. The Puckering Inversion Barrier and Vibrational Spectrum of Cyclopentene. A Scaled Quantum Mechanical Force Field Algorithm. *J. Am. Chem. Soc.* **1992**, *114*, 6834–6849.

(100) Stoppa, P.; Pietropolli Charmet, A.; Giorgianni, S.; Ghersetti, S.; Gambi, A. Tunable Diode Laser Spectroscopy of cis-1,2-Difluoroethylene: Rovibrational Analysis of the ν_9 and $\nu_5+\nu_{10}$ Bands and Anharmonic Force Field. *J. Phys. Chem. A* **2003**, *107*, 474–479.

Figure Captions

Figure 1. Molecular structure of $BrFC=CH_2$: the *a* and *b* principal axes of inertia are in the molecular plane, the *c* axis is perpendicular to it.

Figure 2. Survey spectra of $BrFC=CH_2$ in the region 6500 – 400 cm^{-1} (resolution = 1.0 cm^{-1}, optical path length = 13.4 cm, room temperature). Trace ***a*** refers to the spectrum recorded using a sample pressure of 2.40 hPa, trace ***b*** to the one measured at a sample pressure of 242.5 hPa; both traces have been displaced for clarity. Only some representative bands are labeled.

Figure 3. IR spectrum of $BrFC=CH_2$ in the region 400 – 300 cm^{-1} (resolution = 1.0 cm^{-1}, optical path length = 16.0 cm, pressure = 10 kPa, room temperature).

Figure 4. IR spectrum of $BrFC=CH_2$ in the region 1800 – 1500 cm^{-1} (resolution = 0.2 cm^{-1}, optical path length = 13.4 cm, room temperature). Trace ***a*** refers to the spectrum recorded using a sample pressure of 2.40 hPa, trace ***b*** to the one measured at a sample pressure of 120.5 hPa.

Figure 5. Absorption cross-section spectrum (resolution = 0.5 cm^{-1}) of $BrFC=CH_2$ in the region 6500 – 400 cm^{-1}. Only some representative bands for each spectral interval are labeled.

Table 1. Equilibrium structural parameters and rotational constants of $BrFC=CH_2$[a]

		CCSD(T)[b]	ΔMP2/CBS(T,Q)[c]	ΔCV(MP2/TZ)[d]	Δ*diff*(MP2/TZ)[e]	Best estimate
C_2–F_1		1.3309	-0.0015	-0.0014	+0.0040	1.3321
C_2=C_3		1.3276	-0.0047	-0.0025	+0.0001	1.3205
C_3–H_4		1.0810	-0.0015	-0.0012	+0.0005	1.0787
C_2–Br_5		1.8756	-0.0134	-0.0022	-0.0041	1.8558
C_3–H_6		1.0776	-0.0013	-0.0011	+0.0008	1.0759
< C_3–C_2–F_1		122.54	-0.08	-0.08	-0.18	122.20
< C_3–C_2–Br_5		125.14	+0.20	+0.03	+0.29	125.66
< C_2–C_3–H_6		120.34	-0.20	+0.01	-0.31	119.85
< C_2–C_3–H_4		119.31	+0.06	+0.05	+0.20	119.63
^{79}Br	A_e	10670.01	+57.25	+37.11	-14.44	10749.94
	B_e	3098.19	+37.02	+6.21	+5.89	3147.32
	C_e	2401.02	+25.12	+5.62	+2.79	2434.54
^{81}Br	A_e	10669.98	+57.25	+37.11	-14.44	10749.91
	B_e	3071.30	+36.71	+6.16	+5.85	3120.02
	C_e	2384.84	+24.97	+5.58	+2.79	2418.18

[a]Bond lengths and angles reported in Å and deg, respectively (see Figure 1 for labeling of the atoms), rotational constants in MHz. [b]CCSD(T) calculations carried out employing the cc-pCVTZ(-PP) basis set within the fc approximation (see text). [c]Correction due to the extrapolation to CBS (see text). [d]Correction due to core-correlation effects. [e]Correction due to the inclusion of diffuse function in the basis set (see text).

Table 2. Ground state rotational and quartic centrifugal distortion constants of $BrFC=CH_2$[a]

		CCSD(T)[b]	CCSD(T)+MP2/CBS[c]	CCSD(T)+CBS+CV(MP2)[d]	Best estimate[e]	Exp[f]
^{79}Br	A_0	10614.28	10671.54	10708.65	10694.21	10676.346(3)
	B_0	3087.38	3124.41	3130.62	3136.51	3105.4342(15)
	C_0	2389.18	2414.29	2419.91	2422.70	2403.1913(12)
	Δ_J	0.576	0.580	0.581	0.585	0.595(8)
	Δ_{JK}	3.485	3.425	3.455	3.525	3.64(4)
	Δ_K	7.184	7.463	7.469	7.521	6.4(4)
	δ_J	0.147	0.149	0.149	0.151	0.1523(19)
	δ_K	3.435	3.431	3.449	3.497	3.15(8)
^{81}Br	A_0	10614.24	10671.49	10708.60	10694.16	10676.307(3)
	B_0	3060.60	3097.31	3103.47	3109.32	3078.4937(14)
	C_0	2373.10	2398.08	2403.65	2406.44	2387.0176(12)
	Δ_J	0.566	0.571	0.572	0.576	0.565(8)
	Δ_{JK}	3.436	3.377	3.406	3.476	3.37(4)
	Δ_K	7.242	7.521	7.528	7.581	8.7(4)
	δ_J	0.144	0.146	0.146	0.148	0.1462(9)
	δ_K	3.395	3.391	3.408	3.456	3.46(6)

[a]Ground state rotational constants (in MHz) obtained by augmenting the equilibrium rotational constants with vibrational corrections at the MP2/cc-pVTZ level (see text), quartic centrifugal distortion constants (Watson *A*-reduction, I^r representation; in kHz). [b]fc-CCSD(T)/cc-pCVTZ(-PP) calculations. [c]fc-CCSD(T)/cc-pVTZ augmented by corrections due to the extrapolation to CBS evaluated at the MP2 level (see text). [d]fc-CCSD(T)/cc-pVTZ+MP2/CBS calculations augmented by corrections due to core-correlation (CV) effects evaluated at the MP2 level (see text). [e]fc-CCSD(T)/cc-pVTZ+MP2/CBS+MP2/CV calculations augmented by corrections due to inclusion of diffuse function in the basis set (see text). [f]Taken from Ref. 56.

Table 3. Harmonic wavenumbers (*Wvn*) and intensities (*I*) of $^{79}BrFC=CH_2$ calculated at each step of the composite scheme described in the text and using different basis sets

		CCSD(T)[a]		ΔMP2/CBS(T,Q)[b]		ΔCV(MP2/TZ)[c]		Δ*diff*(MP2/TZ)[d]		Best estimate	
Mode	Sym.[e]	*Wvn*[f]	*I*[f]	*Wvn*[f]	*I*[f]	*Wvn*[f]	*I*[f]	*Wvn*[f]	*I*[f]	*Wvn*[f]	*I*[f]
ω_1	A'	3296.73	0.31	+1.06	+0.53	+5.50	+0.06	-8.24	+0.06	3303.28	0.91
ω_2	A'	3184.90	2.26	-2.53	+0.83	+5.66	+0.14	-6.96	+0.28	3188.03	3.23
ω_3	A'	1696.11	107.86	-1.77	-0.95	+5.51	+0.16	-8.39	-1.35	1699.85	107.07
ω_4	A'	1411.58	2.86	-9.36	-1.28	+2.09	-0.12	-9.95	-0.70	1404.31	1.46
ω_5	A'	1201.71	173.18	-10.87	-1.13	+3.24	-1.02	-13.80	-3.63	1194.09	171.03
ω_6	A'	966.10	35.01	-5.62	+4.55	+1.73	-0.14	-7.23	+4.93	962.20	39.42
ω_7	A'	623.32	31.53	+6.42	-1.05	+1.73	-0.96	-1.17	-1.57	631.47	29.52
ω_8	A'	365.57	0.61	+2.40	+0.17	+1.10	+0.03	-1.45	+0.09	369.07	0.81
ω_9	A'	321.48	0.13	+4.80	+0.12	+0.34	+0.01	-2.77	+0.10	326.62	0.25
ω_{10}	A"	853.91	53.09	+5.29	-6.62	+6.30	+0.24	-7.55	-5.07	865.50	46.71
ω_{11}	A"	724.29	0.29	+0.63	-0.09	+2.73	-0.01	-3.15	-0.03	727.64	0.19
ω_{12}	A"	487.56	1.45	+1.84	+1.39	+2.93	+0.13	-4.26	+1.58	492.32	2.97

[a]CCSD(T) calculations carried out employing the cc-pCVTZ(-PP) basis set within the fc approximation (see text). [b] Correction due to the extrapolation to CBS (see text). [c] Correction due to core-correlation effects. [d]Correction due to the inclusion of diffuse function in the basis set (see text). [e]Symmetry. [f]Wavenumber (*Wvn*) and intensity (*I*) reported in cm^{-1} and km mol^{-1}, respectively.

Table 4. Harmonic wavenumbers (*Wvn*) and intensities (*I*) of $^{81}BrFC{=}CH_2$ calculated at each step of the composite scheme described in the text and using different basis sets

		CCSD(T)[a]		ΔMP2/CBS(T,Q)[b]		ΔCV(MP2/TZ)[c]		Δ*diff*(MP2/TZ)[d]		Best estimate	
Mode	Sym.[e]	*Wvn*[f]	*I*[f]	*Wvn*[f]	*I*[f]	*Wvn*[f]	*I*[f]	*Wvn*[f]	*I*[f]	*Wvn*[f]	*I*[f]
ω_1	A'	3296.73	0.31	1.06	0.53	5.50	0.06	-8.24	0.06	3303.28	0.91
ω_2	A'	3184.90	2.26	-2.53	0.83	5.66	0.14	-6.96	0.28	3188.03	3.23
ω_3	A'	1696.10	107.85	-1.77	-0.95	5.51	0.16	-8.39	-1.35	1699.84	107.06
ω_4	A'	1411.58	2.85	-9.36	-1.28	2.09	-0.12	-9.95	-0.70	1404.31	1.46
ω_5	A'	1201.69	173.14	-10.87	-1.13	3.24	-1.02	-13.80	-3.63	1194.06	170.99
ω_6	A'	966.10	35.02	-5.62	4.55	1.73	-0.14	-7.23	4.93	962.20	39.42
ω_7	A'	623.70	31.54	6.37	-1.04	1.73	-0.96	-1.19	-1.57	630.81	29.53
ω_8	A'	364.30	0.59	2.43	0.16	1.09	0.03	-1.43	0.09	367.82	0.78
ω_9	A'	321.12	0.13	4.79	0.12	0.34	0.01	-2.77	0.10	326.25	0.25
ω_{10}	A"	853.91	53.09	5.29	-6.62	6.30	0.24	-7.55	-5.07	865.50	46.71
ω_{11}	A"	724.28	0.29	0.63	-0.09	2.73	-0.01	-3.15	-0.03	727.64	0.19
ω_{12}	A"	487.49	1.45	1.83	1.39	2.93	0.13	-4.26	1.57	492.26	2.97

[a]CCSD(T) calculations carried out employing the cc-pCVTZ(-PP) basis set within the fc approximation (see text). [b] Correction due to the extrapolation to CBS (see text). [c] Correction due to core-correlation effects. [d]Correction due to the inclusion of diffuse function in the basis set (see text). [e]Symmetry. [f]Wavenumber (*Wvn*) and intensity (*I*) reported in cm^{-1} and km mol^{-1}, respectively.

Table 5. Symmetry adapted internal coordinates of $BrFC=CH_2$(in terms of internal coordinates) employed of the total energy distribution analysis

Symmetry Species	Symmetry adapted internal coordinates	Description in term of internal coordinates[a]
A'	S_1	$\frac{1}{\sqrt{2}}(r_{34} + r_{36})$
	S_2	r_{23}
	S_3	r_{12}
	S_4	r_{25}
	S_5	$\frac{1}{\sqrt{2}}(\alpha_{234} + \alpha_{236})$
	S_6	$\frac{1}{\sqrt{2}}(r_{34} - r_{36})$
	S_7	$\frac{1}{\sqrt{2}}(\alpha_{234} - \alpha_{236})$
	S_8	α_{123}
	S_9	α_{325}
A"	S_{10}	$\frac{1}{\sqrt{2}}(\gamma_{4326} + \gamma_{6342})$
	S_{11}	$\frac{1}{\sqrt{2}}(\gamma_{1235} + \gamma_{5213})$
	S_{12}	$\frac{1}{\sqrt{2}}(\tau_{1234} + \tau_{5236})$

[a]See text for labeling.

Table 6. Total Energy Distribution (TED%) analysis for each normal mode of $BrFC=CH_2$ and its corresponding approximate description in terms of symmetry-adapted internal coordinates

Mode	TED%	Approximate description	Wavenumber (cm^{-1})
ω_1	S_6(98)	anti-sym. CH_2 stretch.	3296.7
ω_2	S_1(97)	symm. CH_2 stretch.	3184.9
ω_3	S_2(76)	C=C stretch.	1696.1
ω_4	S_5(86)	CH_2 scissors	1411.6
ω_5	S_3(42) + S_7(31)	C-F stretch./ CH_2 rock	1201.7
ω_6	S_7(52) + S_3(39)	CH_2 rock/ C-F stretch.	966.1
ω_7	S_4(49) + S_8(34)	C-Br stretch./ C=C-F bending	623.3
ω_8	S_8(59) + S_4(41)	C=C-F bending/ C-Br stretch.	365.6
ω_9	S_9(104)	C=C-Br bending	321.5
ω_{10}	S_{10}(102)	CH_2 wag	853.9
ω_{11}	S_{12}(94)	torsion	724.3
ω_{12}	S_{11}(95)	C=CBrF out-of-plane	487.6

TABLE 7. Summary of the assigned overtones, combination and hot bands (cm^{-1}) from the gas-phase infrared spectra of $BrFC=CH_2$

Band	Wavenumber[a] /cm^{-1}	Band	Wavenumber[a] /cm^{-1}	Band	Wavenumber[a] /cm^{-1}
$\nu_9+\nu_{12}-\nu_8$	432.5(3)	$\nu_3+\nu_8$	2008(1)	$\nu_1+\nu_{10}$	3978.2(5)
$\nu_{10}-\nu_9$	515.0 (5)	$\nu_5+\nu_6$	2109.0(5)	$\nu_2+\nu_6$	4014.5(3)
$2\nu_8$	735.3(3)	$\nu_3+\nu_{12}$	2117.9(1)	$\nu_1+\nu_6$	4094.8(5)
$\nu_8+\nu_{12}$	840.7(1)/840.1(1) [b]	$\nu_3+\nu_9+\nu_{12}$	2446.3(3)	$\nu_2+\nu_5$	4230.4(3)
$2\nu_8+\nu_{12}-\nu_9$	892.4(3)	$\nu_4+\nu_5$	2532.3(3)	$\nu_1+\nu_5$	4318.3(3)
$\nu_4-\nu_8$	1004.8(3)	$\nu_3+\nu_6+\nu_9-\nu_8$	2543(1)	$\nu_3+2\nu_4$	4391.2(5)
$\nu_4-\nu_9$	1047.8(3)	$\nu_3+\nu_6$	2589(1)	$\nu_2+\nu_4$	4427.8(5)
$\nu_{11}+\nu_{12}$	1183.6(1)	$\nu_5+\nu_7+\nu_{10}$	2622(1)	$2\nu_3+\nu_5$	4446.6(3)
$2\nu_7$	1236.2(3)/1235.0(3) [b]	$2\nu_5+\nu_9$	2643.4(5)	$\nu_1+\nu_4$	4503.5(5)
$\nu_{10}+\nu_{12}$	1308.7(3)	$\nu_3+\nu_4-\nu_9$	2681.5(5)	$\nu_2+\nu_5+\nu_9$	4556.8(3)
$\nu_6+\nu_8$	1310.7(5)/1309.4(5) [b]	$\nu_5+\nu_6+\nu_7$	2720.0(5)	$\nu_2+\nu_3$	4672.6(3)
$\nu_7+2\nu_8$	1338.1(3)	$2\nu_4$	2729.8(3)	$\nu_2+2\nu_{10}$	4701.3(3)
$\nu_4+\nu_9-\nu_9$	1372.5(3)	$\nu_4+2\nu_{11}$	2771.1(5)	$\nu_2+\nu_4+\nu_9$	4742.2(3)
$\nu_6+\nu_{12}$	1420.8(1)	$\nu_3+\nu_5$	2809.0(3)	$\nu_1+2\nu_{10}$	4791.4(5)
$\nu_5+\nu_9$	1487.6(9)	$\nu_3+\nu_4$	3001.2(5)	$\nu_1+\nu_3$	4823.9(3)
$\nu_{10}+\nu_{11}$	1542(1)	$\nu_5+2\nu_6$	3046.6(3)	$\nu_2+\nu_5+\nu_7$	4825.4(3)
$\nu_6+\nu_7$	1563(1)	$\nu_3+2\nu_{11}$	3068.9(3)	$\nu_1+\nu_3+\nu_6$	5777.2(5)
$2\nu_{10}$	1692.0(5)	$2\nu_3$	3277.9(3)	$\nu_2+\nu_3+\nu_5$	5820.4(5)
$\nu_4+\nu_8$	1732.7(3)/1731.5(3) [b]	$\nu_3+\nu_4+\nu_9$	3324.1(3)	$\nu_1+2\nu_4$	5846.4(5)
$\nu_5+\nu_7$	1782(1)	$\nu_4+\nu_5+\nu_{10}$	3366.9(5)	$2\nu_2$	6021.4(3)
$\nu_5+\nu_{11}$	1874(1)	$\nu_2+\nu_9$	3389.7(5)	$\nu_2+\nu_3+\nu_4$	6061.2(5)
$2\nu_6$	1895.5(3)	$\nu_1+\nu_9$	3474.9(5)	$\nu_1+\nu_2$	6094.5(5)
$\nu_3+\nu_9$	1967(1)	$\nu_3+\nu_5+\nu_6$	3752.5(5)	$\nu_1+\nu_3+\nu_4$	6147.5(5)
$\nu_4+\nu_7$	1985.5(3)/1984.8(5) [b]	$\nu_1+\nu_7$	3770.5(5)	$2\nu_1$	6260.4(3)

[a]The experimental error in parentheses is on the last significant digit. [b]$^{79/81}$Br isotopologues.

TABLE 8. Comparison between the observed and calculated gas-phase infrared frequency fundamentals (cm^{-1}) of $BrFC=CH_2$

			HYB-1[a]				HYB-2[b]			
			GVPT2[c]		HDCPT2[d]		GVPT2[c]		HDCPT2[d]	
Band	Symmetry	Observed[e]	Calculated[e,f]	Δ[e,g]	Calculated[e,f]	Δ[e,g]	Calculated[e,f]	Δ[e,g]	Calculated[e,f]	Δ[e,g]
ν_1	A'	3154.3(3)	3161.14	-6.8	3160.1	-5.8	3164.0	-9.7	3163.0	-8.7
ν_2	A'	3068.7(3)	3067.4*	1.3	3063.1	5.6	3072.3*	-3.6	3065.0	3.7
ν_3	A'	1647.3(1)	1647.8*	-0.5	1652.1	-4.8	1653.6*	-6.3	1654.6	-7.3
ν_4	A'	1368.6(3)	1366.7*	1.9	1364.7	3.7	1371.4*	-2.8	1369.0	-0.4
ν_5	A'	1168.5(1)	1167.8	0.7	1167.8	0.7	1168.6	-0.1	1168.7	-0.2
ν_6	A'	946.4(1)	939.8*	6.6	946.2	0.2	940.6*	5.8	947.1	-0.5
ν_7	A'	617.8(1)/617.3(1)[h]	623.4	-5.6	623.5	-5.7	624.4	-6.6	624.4	-6.6
ν_8	A'	364.0(5)/362.6(5)[h]	366.7	-2.7	366.7	-2.7	367.0	-3.0	367.0	-3.0
ν_9	A'	321.1(5)	325.2	-4.1	325.2	-4.1	325.3	-4.2	325.3	-4.2
ν_{10}	A"	839.0(1)	841.6	-2.6	843.4	-4.4	846.0	-7.0	847.6	-8.6
ν_{11}	A"	707.8(1)	710.3	-2.5	710.9	-3.1	712.2	-4.4	712.9	-5.1
ν_{12}	A"	476.1(1)	485.2	-9.1	485.2	-9.1	485.5	-9.4	485.5	-9.4

[a]HYB-1 refers to the hybrid force field obtained from the *best-estimated* harmonic data augmented by anharmonic force constants calculated at the MP2/cc-pVTZ(-PP) level of theory (see text). [b]HYB-2 refers to the hybrid force field obtained from the *best-estimated* harmonic data augmented by anharmonic force constants calculated at the B2PLYP/cc-pVTZ(-PP) level of theory (see text). [c]Generalized second-order Vibrational Perturbational Theory, see Ref. 88. [d]Hybrid Degeneracy-Corrected second-order Perturbation Theory, see Ref. 92. [e]All the values in cm^{-1}. [f]Values marked by an asterisk are computed taking into account anharmonic resonances (see discussion in the text). [g]Observed – Calculated. [h]$^{79/81}$Br isotopologues.

Table 9. Integrated absorption cross sections (km mol^{-1}) of $BrFC=CH_2$

Integration limits / cm^{-1}	***Experimental***[a]	HYB-1[b]	HYB-2[c]
440 – 520	2.43(1)	2.97	2.90
580 – 650	31.9(6)	30.11	30.32
700 – 720	0.50(2)	0.16	0.14
720 – 750	0.39(1)	0.17	0.20
780 – 900	46.1(2)	45.23	45.83
900 – 1000	45.02(9)	41.78	42.27
1090 – 1210	169.9(5)	161.45	163.33
1210 – 1270	5.75(5)	6.43	5.39
1280 – 1340	1.52(3)	1.57	1.40
1340 – 1400	1.82(4)	0.48	0.63
1460 – 1500	0.20(6)	0.12	0.12
1500 – 1750	107.2(5)	112.19	118.01
1750 – 1800	0.60(7)	0.89	0.79
1830 – 1940	1.7(1)	1.84	2.29
1940 – 1980	0.37(1)	0.19	0.17
2040 –2180	1.42(3)	1.45	1.49
2430 – 2680	1.51(3)	2.09	1.49
2680 – 2750	0.133(4)	0.37	0.29
2750 – 2900	0.73(2)	0.77	0.80
2910 – 3190	2.16(6)	2.07	2.57
3200 – 3360	1.37(3)	1.90	1.54
3360 – 3450	0.11(1)	0.09	0.08
3450 – 3500	0.03(1)	0.05	0.04
3955 – 4045	0.03(1)	0.27	0.23
4045 – 4135	0.17(1)	0.38	0.35
4135 – 4270	0.27(1)	0.68	0.77
4270 – 4375	0.49(1)	0.52	0.58
4375 – 4600	0.39(1)	1.33	1.30
4600 – 4760	0.83(1)	0.13	0.09
4770 – 4850	0.04(1)	0.07	0.07
5920 – 6200	0.79(1)	0.67	0.88
6200 – 6320	0.47(1)	0.64	0.85

[a]Figures in parenthesis are one standard deviation in units of the last significant digits. [b]HYB-1 refers to the hybrid force field obtained from the *best-estimated* harmonic data augmented by anharmonic force constants calculated at the MP2/cc-pVTZ(-PP) level of theory (see text). [c]HYB-2 refers to the hybrid force field obtained from the *best-estimated* harmonic data augmented by anharmonic force constants calculated at the B2PLYP/cc-pVTZ(-PP) level of theory (see text).

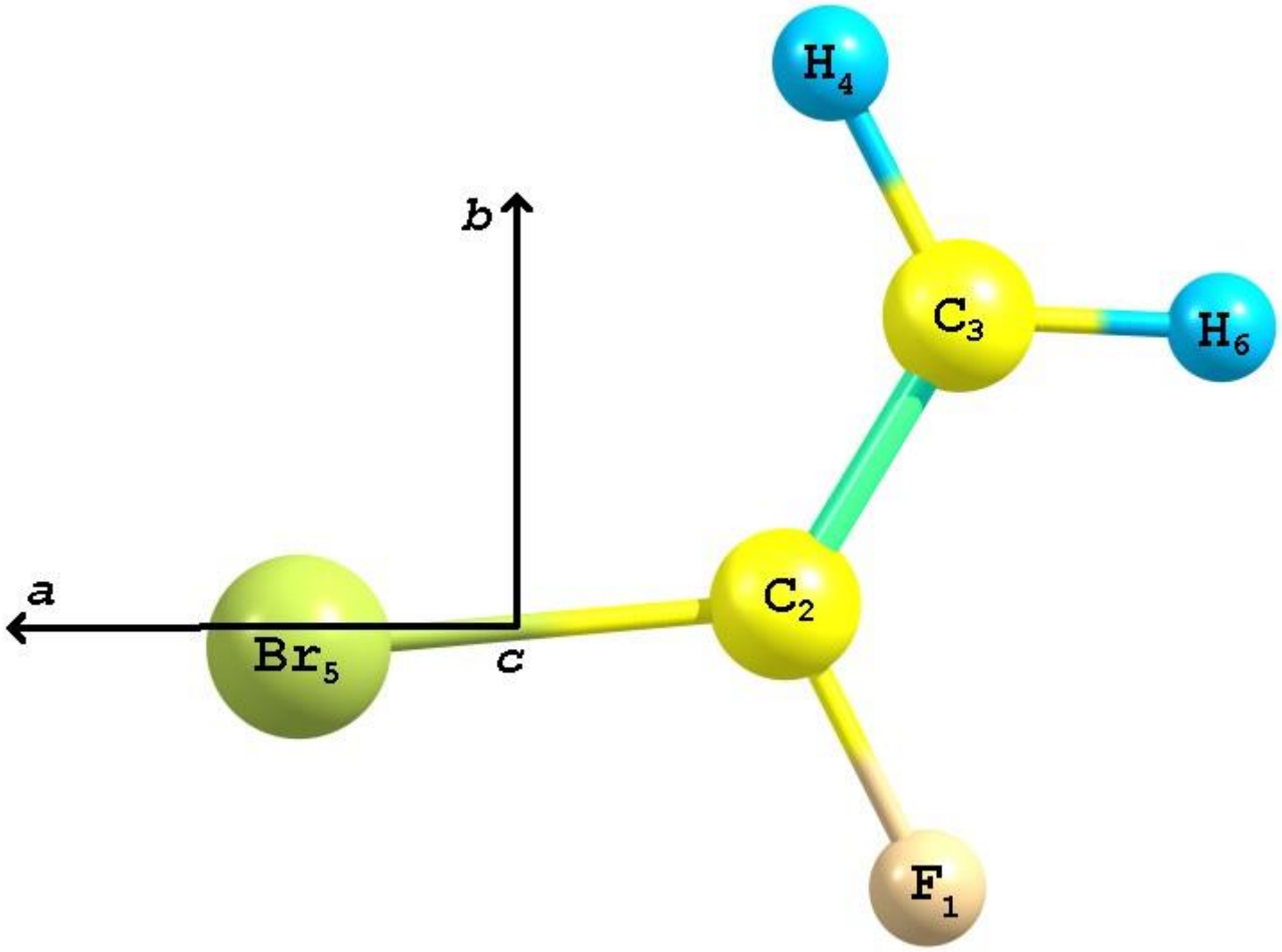

Figure 1

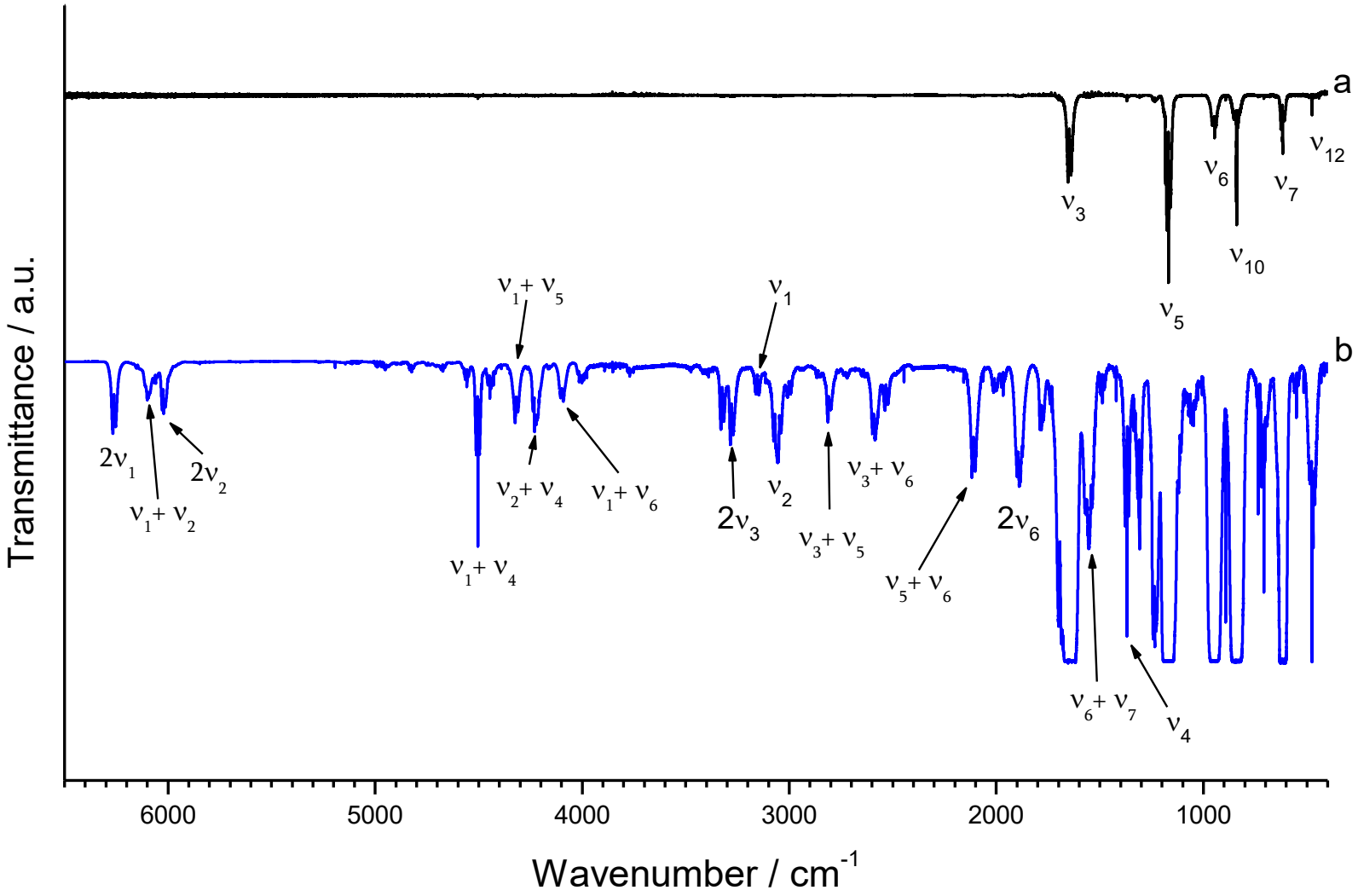
Transmittance / a.u.
Wavenumber / cm-1
6000
5000
4000
3000
2000
1000
a
b
ν3
ν5
ν6
ν7
ν10
ν12
ν1 + ν5
ν1
2ν1
2ν2
ν1 + ν2
ν2 + ν4
ν1 + ν6
ν1 + ν4
2ν3
ν2
ν3 + ν6
ν3 + ν5
ν5 + ν6
2ν6
ν6 + ν7
ν4

Figure 2

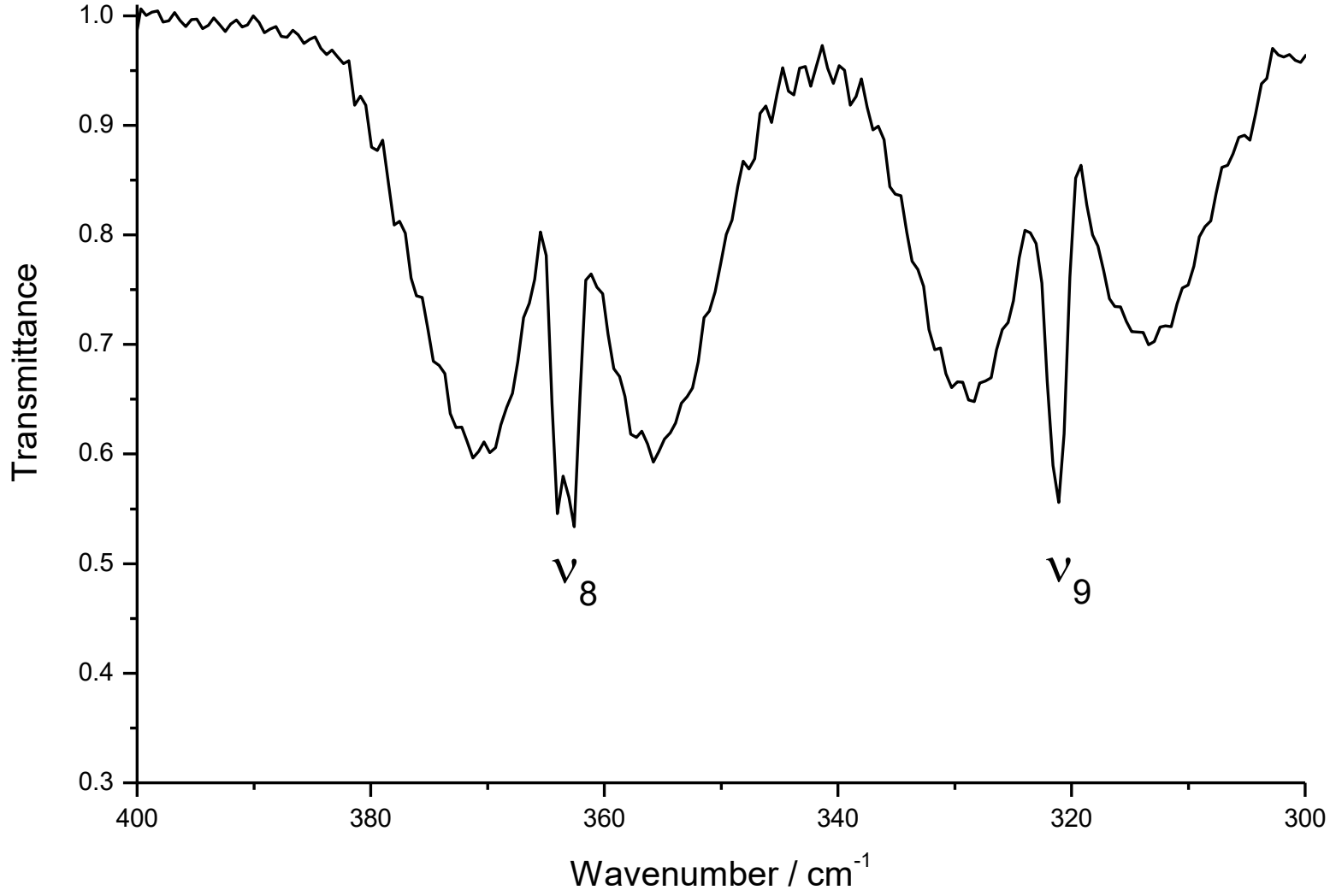
Transmittance
1.0
0.9
0.8
0.7
0.6
0.5
0.4
0.3
400
380
360
340
320
300
Wavenumber / cm-1
ν8
ν9

Figure 3

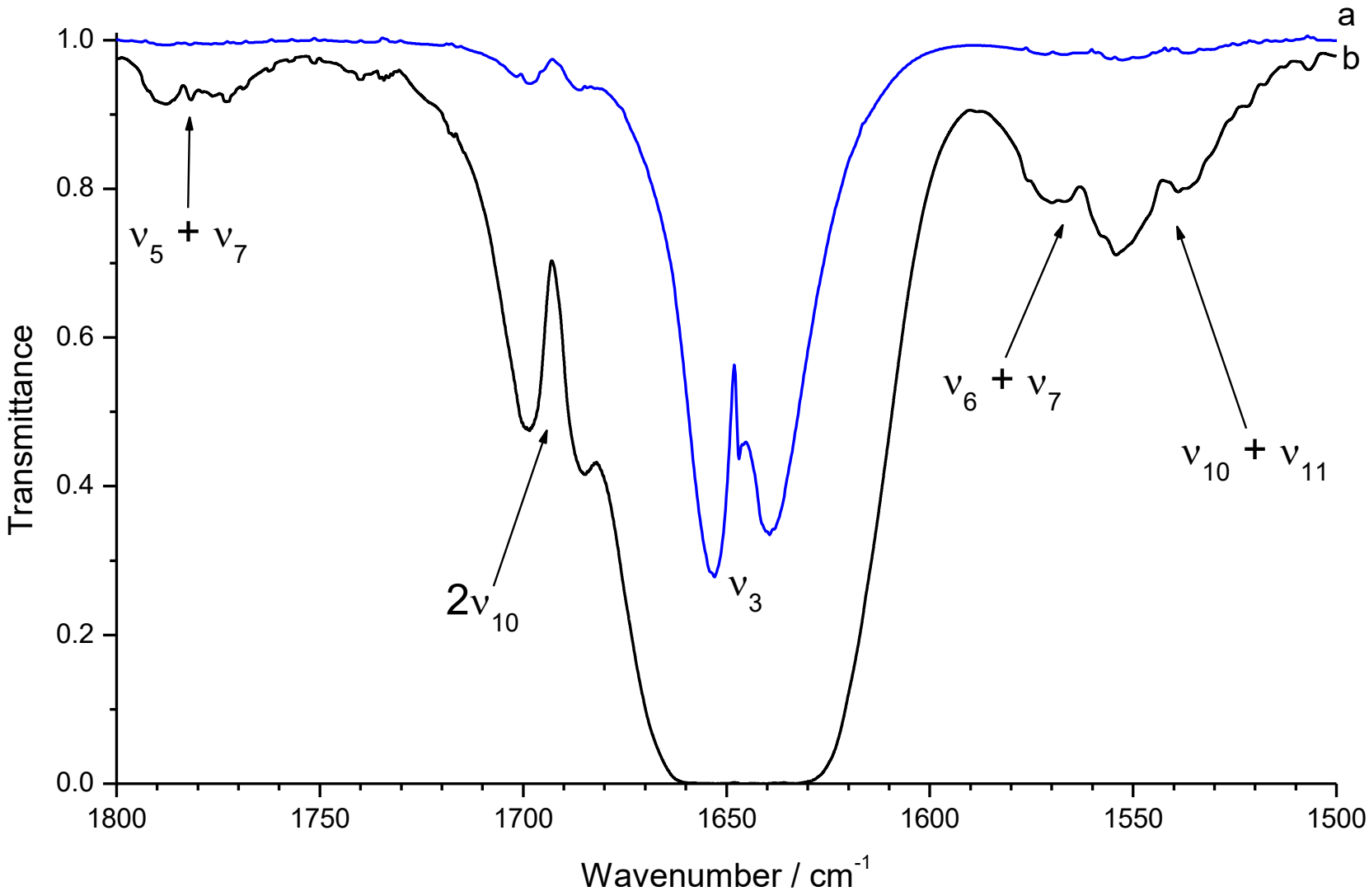
a
b
1.0
0.8
0.6
0.4
0.2
0.0
Transmittance
1800
1750
1700
1650
1600
1550
1500
Wavenumber / cm-1
ν5 + ν7
2ν10
ν3
ν6 + ν7
ν10 + ν11

Figure 4

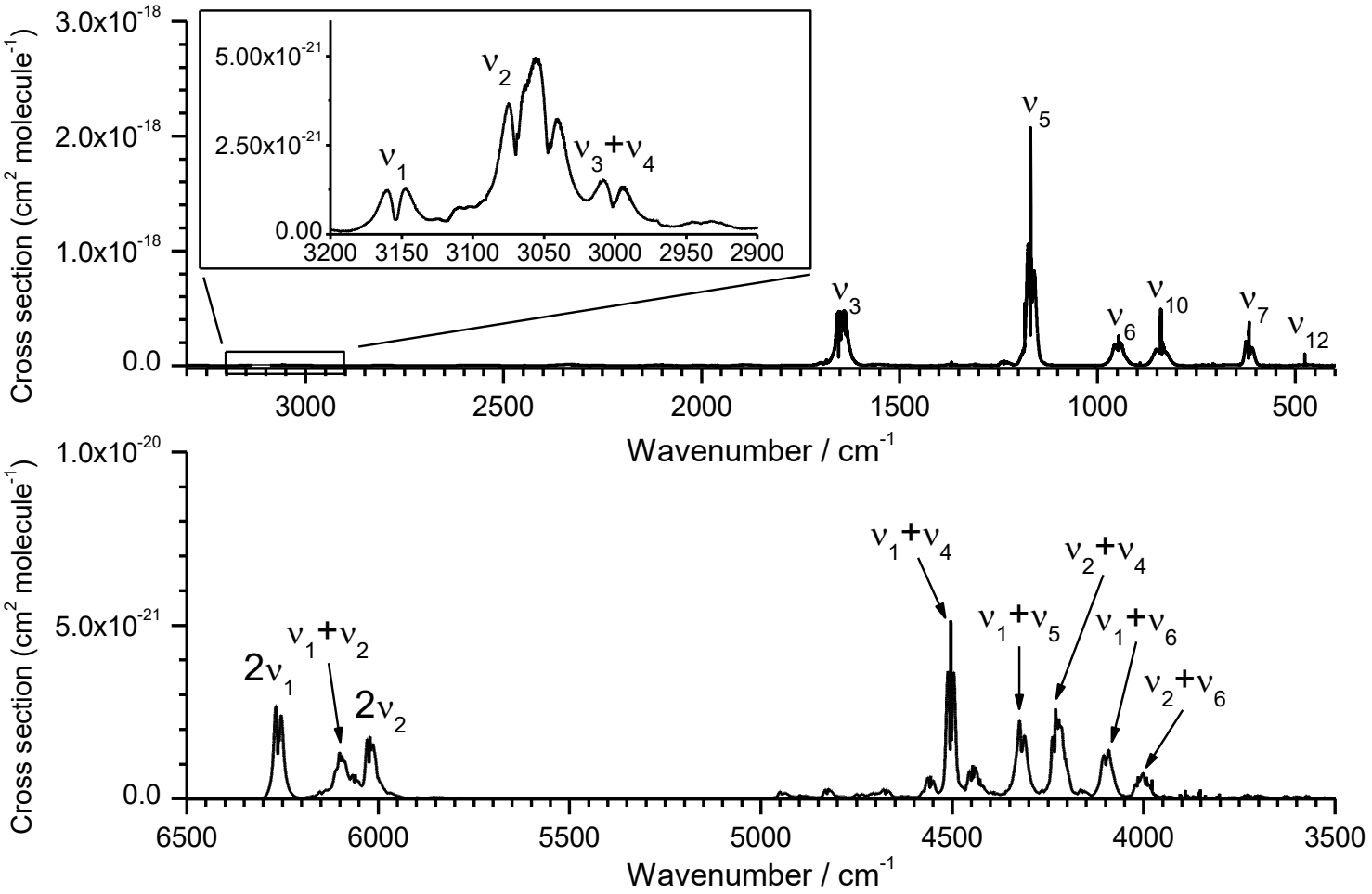
Cross section (cm^2 molecule^{-1})
3.0x10^{-18}
2.0x10^{-18}
1.0x10^{-18}
0.0
5.00x10^{-21}
2.50x10^{-21}
0.00
3200 3150 3100 3050 3000 2950 2900
ν_1
ν_2
$\nu_3+\nu_4$
ν_3
ν_5
ν_6
ν_{10}
ν_7
ν_{12}
3000 2500 2000 1500 1000 500
Wavenumber / cm^{-1}
Cross section (cm^2 molecule^{-1})
1.0x10^{-20}
5.0x10^{-21}
0.0
$2\nu_1$
$\nu_1+\nu_2$
$2\nu_2$
$\nu_1+\nu_4$
$\nu_2+\nu_4$
$\nu_1+\nu_5$
$\nu_1+\nu_6$
$\nu_2+\nu_6$
6500 6000 5500 5000 4500 4000 3500
Wavenumber / cm^{-1}

Figure 5

TOC Graphic

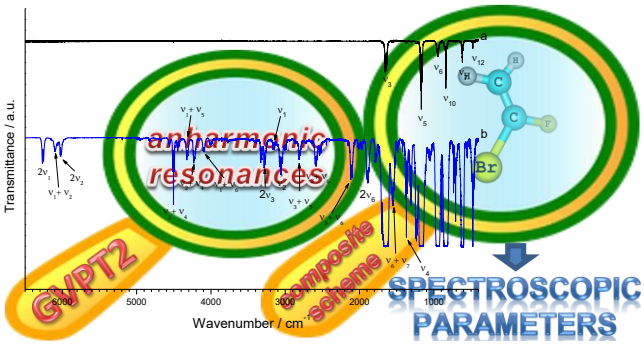
Transmittance / a.u.
Wavenumber / cm⁻¹
5000
4000
3000
2000
1000
anharmonic resonances
VPT2
composite scheme
SPECTROSCOPIC PARAMETERS
Br